



NUCLEAR ENERGY INSTITUTE

**Lynnette Hendricks**  
DIRECTOR, LICENSING  
NUCLEAR GENERATION

August 16, 2001

M. Wayne Hodges  
Deputy Director  
Spent Fuel Project Office  
U.S. Nuclear Regulatory Commission  
MS 0-13 D13  
Washington, DC 20555-0001

Dear Mr. Hodges,

Attached please find industry's responses to the set of RAIs that NRC provided following our meeting on April 18, 2001. This public meeting was held to address NRC comments on the two EPRI reports submitted to NRC. The first report was submitted late in 2000 (Creep as the Limiting Mechanism) and the second was submitted in January 2001 (Fracture Toughness of High Burnup Fuel).

As you will see a large amount of effort was included in responding to the RAI's in a thoughtful, comprehensive manner. I believe the discussions and formal responses to the RAIs achieve the objectives of the April 18 meeting of establishing a clear understanding of existing data and the technical basis underlying industry's approach to storing high burnup fuel. Per our previous commitment, we will be submitting the third report, which translates the technical bases for evaluating dry storage conditions into a model and criteria for conservatively limiting cladding creep during storage to acceptable levels, by September 14, 2001.

I will contact you after you receive the third report to schedule a public meeting. If you have any questions as you review the attachment, please call me at 202-739-8109.

Sincerely,

Lynnette Hendricks

Attachment: Response to NRC's RAI Letter, Dated May 18, 2001, Regarding High Burnup Fuel Characteristics, August 10, 2001

2046



**Response to NRC's RAI Letter, Dated May 18, 2001,  
Regarding High Burnup Fuel Characteristics**

**August 10, 2001**

## Section A: General

***A-1. Using appropriate stress analyses that model normal handling operations, demonstrate that high burnup fuel assemblies can be retrieved intact from the storage cask system or Independent Spent Fuel Storage Installation at the end of the licensing period. In the response, include the effects of creep damage and any potential wall thinning that could occur during the licensing period. Evaluate the likelihood and consequences of potential fuel cladding failure during retrieval operations of the fuel from the storage cask. The analysis should assume that the failed high burnup fuel redistributes in a credible, but bounding configuration.***

Excluding accidental drops and transportation-related loads, which are outside the present scope, retrieval operations of high burnup fuel assemblies from the storage cask system at the end of the licensing period do not subject the fuel assemblies to higher loads than handling operations prior to placement in dry storage casks. The only change in fuel conditions during in-cask storage, which would require re-evaluation, is the effect of cladding creep deformations and consequential wall thinning on the cladding resistance to bending that may be caused by handling loads. The primary measure of the bending stiffness of the cladding is the moment of inertia, which, for an empty tube disregarding the stiffening effect of the fuel, is given by the expression,  $I = (\pi/4) (r_0^4 - r_i^4) \cong \pi r^3 t$ , where  $r$  is the cladding mean radius and  $t$  is the thickness. A simple substitution of the effect of creep strain on  $r$  and  $t$  would show that the moment of inertia becomes larger for any amount of creep strain. Hence, the cladding resistance to bending is enhanced rather than degraded by creep, provided no creep rupture occurs during dry storage.

Treating creep rupture as a faulted condition that should be prevented, implicitly renders the consequences of creep rupture on handling operation and retrieval totally avoidable. The potential for the cladding to creep-rupture during in-cask dry storage is discussed in a recent paper accepted for presentation at the upcoming ICEM01 Conference (Attachment 2), and will be discussed in greater detail in the third Industry Report on Creep Methodology. It is shown that creep rupture is a condition of plastic instability, which is possible only at the ultimate tensile strength of the material. Therefore, a sure method of avoiding creep rupture is to prevent the cladding stress from rising above the yield strength. As will be shown in the references cited above, the peak cladding stress, even in local regions of hydride lenses, is a fraction of the yield stress. Other considerations that come into play regarding cladding failure, such as, for example, the question of radial hydrides, were addressed in EPRI Report 1001207, and will be discussed further in this document.

## **Section B: EPRI Report 1001207, "Creep As The Limiting Mechanism For Spent Fuel Dry Storage", December 2000**

**B-1. The report outlines an approach that establishes a creep strain limit. Describe the methodology that a licensee would use to derive a temperature limit, or other licensee/cask vendor controllable limit from the proposed creep strain limit, that would demonstrate that 10 CFR 72 regulations are met. Provide example predictions of peak fuel cladding temperature limits for high burnup fuel at the limiting stresses. Also, provide the corresponding creep strain predictions.**

This information will be provided in the upcoming report on Creep, which is the third companion report to the two reports addressed in the referenced NRC's RAI.

**B-2. The report concludes that stresses in excess of 138 MPa and several thermal cycles are needed to obtain significant hydride reorientation to cause delayed hydride cracking of spent fuel during dry storage. Justify how the data of Louthan and Marshall (1963), Hindle and Slattery (1971), Ells (1968) and Pickman (1972), and Einziger and Kohli (1984) support this conclusion.**

The reference to the 138 MPa and thermal cycling in the EPRI report is not, as indicated in the RAI, a conclusion statement, but rather a description of Simpson's findings, reference 60 in the Report. The Report states on page 3-5, "*Simpson et al. found that a stress in excess of 138 MPa was required, and the degree (number and angle) of re-orientation was strongly dependent on the number of cycles, with tens of cycles required to produce significant re-orientation*".

The EPRI Report quotes appropriate references for stress and temperature ranges for the DHC mechanism, and ends with two major conclusions that do not seem to be at variance with the references cited in the RAI, (see report conclusions (4) and (5) in the main conclusions section, Chapter 6). The Einziger and Kohli results are for hoop stresses above 145 MPa, which fall in the 120-180 MPa value quoted in the EPRI Report. Einziger and Kohli also state that for DHC to be ruled out on the basis of hydride re-orientation, the temperature has to drop below 305°C. The EPRI Report, on the other hand, does not rule out hydride re-orientation at lower temperatures if the stresses are sufficiently high. For example, at 250°C stresses in the range 250-350 MPa are required to cause hydride re-orientation. In all expected cases, these stress levels are inconsistent with spent fuel rods at 250°C.

The remaining references cited in the RAI document deal with the effects of manufacturing methods of Zircaloy-2 tubing on hydride precipitation. Different manufacturing processes lead to different crystallographic textures, which in turn lead to different susceptibilities to hydride re-orientation, depending upon the degree of orientation of the basal plane normals relative to the applied stress. In his survey article, Ells (1968) argues that the results of Louthan and Marshall (1962) and Hindle and Slattery (1966), could be used to manufacture Zircaloy tubing with lower susceptibility to unfavorable hydride precipitation by simply changing the sequence and direction of tube reduction steps.

The effect of texture on hydrides orientation is to change the stress levels at which hydrides can precipitate in the radial direction in pressurized Zircaloy tubes. As is well known, CWSR Zr-4 cladding has strong radial texture compared to annealed Zr-2, and is much less susceptible than Zr-2 to radial hydrides precipitation, [2]. As quoted in the EPRI Report, at temperatures typical of dry storage temperatures, stresses above 120 MPa are needed for radial hydrides precipitation. It should be

mentioned, however, that we have very recently come across limited unpublished data (one example), which indicates that the stress threshold for hydride re-orientation can be of the order of 90 MPa at temperatures above 415°C. This new information, however, does not invalidate the Report's conclusions regarding DHC (see the discussion below).

The above discussion on hydrides re-orientation, in response to the issue raised in the RAI document, is made redundant by the fact that the EPRI Report contains a detailed analysis of the DHC consequences of a radial crack. The effects are the same regardless of whether the crack had pre-existed (from PCI) or had initiated from a radial hydride during storage. The discussion on pages 3-3 to 3-7 of the Report gives an analysis of DHC consequences of a radial crack assumed to be in the worst possible location, namely, in the ligament beneath a hydride lens. The analysis shows that a radial crack of 55 µm, which was shown to be the largest crack size that could pre-exist in a fuel rod with spalled oxide, in a ligament under 265 MPa stress remains sub-critical with respect to DHC initiation. It should be noted that at temperatures above the ductile-brittle transition, ~150-200°C, the hydrides remain ductile.

Inter-linkage of radial hydrides, forming potential crack sites, is not observed under slow cooling typical of dry storage. The unusually long radial hydrides observed by Einziger and Kohli after fast pressurized cooldown from 323°C is most likely due to the sudden drop in the solubility limit, which released a large amount of hydrogen at once. The results contradict Einziger et al. whole-rod tests cooled at ~10°C/h, *Nucl. Technol.*, 57, 65 (1982). The difference in behavior was attributed to the cooldown rate. During dry storage, the rate of precipitation of radial hydrides is a function of the drop in the solubility limit with temperature, which is no more than a few ppm per month. It would seem, therefore, that postulating a worst case combination of high local stress with massive radial hydrides is not a statistically significant condition, and diverts attention from more realistic safety concerns.

***B-3. The report claims that the high burnup and highly oxidized/hydrided (and spalled) Zircaloy has sufficient fracture toughness to withstand crack propagation. Justify that the fracture toughness values (used in the calculations) are applicable to highly oxidized Zircaloy cladding (including spalled cladding) that is typical of highly burned fuel.***

***B-4. Provide the justification for selecting the critical strain energy density (CSED) approach as a method to predict the fracture toughness of Zircaloy cladding of high burnup fuel. In the absence of data, a discussion of the applicability of this method to materials with conditions similar to Zircaloy clad high burnup fuel and a comparison of appropriate data to modeling predictions should be provided.***

EPRI Report 1001281 describes the state of the art of fracture toughness data for Zircaloy, which, with one exception, is limited to plane strain specimens. The one exception is the Gregoriev et al. (ASTM STP 1295) test, which is not an ASTM-approved test. Testing of cladding geometry continues to evolve, (see Rashid et al., "Evaluation of Fracture Initiation and Extension in Fuel Cladding", Proceedings of Park City Meeting, p151). Also, the EPRI-managed NFIR Program is sponsoring a round-robin program for fracture toughness tests using cladding geometry. Until such time when the state of the art of fracture toughness testing matures to the point where reliable data is produced for high burnup cladding with spalled oxide, we must rely on correlation techniques to derive conservative estimates of fracture toughness. This is the primary motivation for the development of the  $K_{IC}$ -CSED correlation, expressed as  $K_{IC} = 3.5 \sqrt{CSED}$ , and its application to spent fuel dry storage is dictated by necessity. As far as can be determined, there is no known alternative model to this correlation, with the possible exception of adapting to high-burnup Zircaloy the  $K_{IC}$ -CVN correlation, (Rolf and Barsom),

developed for high strength steels. This clearly requires Charpy upper-shelf V-notch data, which is lacking for high-burnup Zircaloy cladding.

Justification of the  $K_{IC}$ -CSED correlation must come from comparing it to  $K_{IC}$  data for non-tube geometry and CSED data for tube geometry. The EPRI Report 1001207, page 3-4, contains a comparison of the analytically-derived  $K_{IC}$  based on Garde et al. data to measured  $K_{IC}$  for hydrogen-charged un-irradiated and irradiated specimens by Kreyns et al., with very good agreement, e.g., 7.8 calculated vs. 7.4 measured. The analysis on page 3-4 of the EPRI Report derives a penalty factor of 3 on the effect of hydrogen on fracture toughness. This penalty factor, when applied to the corrosion-hydrogen concentration, gives the equivalent effect of a charged-hydrogen concentration on fracture toughness. For example, a fuel cladding with 500-ppm hydrogen concentration would have similar fracture toughness to that obtained from a hydrogen-charged specimen with 1500-ppm hydrogen concentration.

The main features of the  $K_{IC}$ -CSED correlation are that it is:

- (a) Developed for semi-brittle material that exhibits limited strain-hardening capabilities and with mechanical properties similar to irradiated Zircaloy. Its application to tensile data for ferritic steels, as shown in Reference 1, extrapolates the correlation beyond its intended application.
- (b) Conservative.
- (c) Particularly suited for rods with spalled oxide and localized hydrides, which exhibit limited ductility and show the lowest values of CSED when tested under internal pressure.

***B-5. One of the major conclusions of the report is that "sufficient data and analytical modeling exist to show that a strain limit of 2% can be safely used as an asymptotic limit for fuel rods normally discharged from reactors without imposing any restrictions on oxide thickness or physical conditions." Provide a discussion, citing references, that describes the data and assumptions that were used to support the 2% strain limit for prototypical high burnup fuel experiencing the stress and temperature ranges expected under dry storage conditions. The expected cladding temperature and stress ranges where creep is expected to be the dominant deformation mechanism under dry cask storage conditions are 300-400°C and 50-150 MPa, respectively. The expected oxide thickness and average hydrogen concentration of high burnup fuel are in the range of 50-130 micrometers and 300-900 parts per million, respectively for non-spalled rods.***

Goll et al. [Reference 61 in Report 1001207] conducted creep experiments using cladding specimens from Zr-4 fuel rods irradiated to 64 MWd/KgU at temperatures of 370°C and 300°C at cladding nominal stresses of 400 and 630 MPa, respectively. (The actual stresses are higher because of the effect of the oxide on the effective wall thickness). While the temperatures are in the range of dry storage, the stresses are significantly higher, by a factor of 3 to 5, compared to initial storage stresses. The creep tests were followed by so-called ductility tests, which were conducted at lower temperatures for a period of five days to determine any loss in ductility due to radial hydride precipitation during cool down under pressure. The lowest failure strains measured outside the rupture region were 3% at 370°C and 410 MPa and 2.5% in a repaired sample tested at 300°C and 630 MPa. These strains were determined by averaging over the intact region, hence they were referred to as "Uniform Plastic Elongation". By conducting such accelerated creep tests, a fundamental change in material behavior was introduced, namely, combining rate-dependent creep with rate-independent plastic flow. No failures occurred in the ductility tests despite the presence of radial hydrides.

A creep rupture test using 4-cycle CWSR Zr-4 cladding carried out by EDF/CEA researchers [Reference 63 in Report 1001207] showed a strain of 10% prior to failure after 42 days of creep at a constant temperature of 420°C and a nominal initial stress of 200MPa. We believe that this specimen had undergone irradiation-damage annealing, and possibly partial recrystallization, early in the test due to the relatively high temperature of 420°C. This test would be an interesting candidate for FALCON analysis, and will be included in the third EPRI report.

This test provides the only available creep “failure” data for irradiated cladding. Although this data supports the use of the 2% strain limit, we do not subscribe to the use of strain alone as a criterion. This is because strain is not a unique response quantity, as it depends on the loading path, and, therefore, is not a sufficient condition for material failure under dry storage conditions. Creep rupture tests conducted at EDF/CEA using un-irradiated hydrided cladding (1000 ppm) show that for creep rupture to occur, the stress has to rise above the yield strength, eventually reaching the condition of plastic instability at the material’s ultimate tensile strength.

In fuel design practice where a strain limit is used as a design criterion, the stress is an implied condition, i.e., PCMI is the primary loading mechanism. Extrapolating such practice to long term creep behavior in dry storage, where the stress state remains in the elastic regime, requires the consideration of both the strain and the stress for the process to be technically sound. The strain data by Garde et al., Reference 55 in the EPRI Report, which may have led to the 1% strain limit in ISG-11, was never intended to stand alone. Unfortunately, Garde et al. did not report in their paper the stresses that went with the strains, but the stress information is contained in EPRI’s hot cell report EPRI TR-103302-V2, Reference 59 in EPRI 1001207, which was used to generate the CSED criterion.

An attempt to re-interpret Garde’s data for creep behavior was described in the EPRI Report 1001207 on pages 4-7 to 4-11. A circumferentially averaged strain limit of 2% is derived, accounting only for strain-rate effects and maintaining the stress above the yield strength. This derivation is in effect an analytical extrapolation of material property tests to creep rupture tests of the type conducted in Germany and France referenced above.

***B-6. Justify the use of total strain (versus uniform strain) to adequately predict, and provide sufficient margin for, the expected failure mode(s) of high burnup fuel cladding under expected dry cask storage conditions. If the NEI/EPRI approach utilizes the total strain as the basis for a strain limit, as proposed in the subject report, describe how the proposed methodology (a) differentiates the strain observed in tensile tests from the strain observed in creep tests, (b) is related to creep phenomena, and (c) uses extrapolation of tensile (residual) strain data to creep strain limit considers the effect of potentially adverse localized cladding microstructural features (such as hydride lenses).***

Much of the above discussion in response to Item B-5 applies here also. First, we must explain, from a continuum mechanics perspective, the meaning of the terms “uniform elongation” and “total elongation.” The latter term is self-explanatory, and the first term describes the “engineering” strain that is measured in a tensile test at the point of maximum load. The implication is that this point is the onset of necking and instability. However, the true-stress, true strain curve is the only material characterization that is used in modeling and analysis, and when the engineering-stress, engineering-strain data is converted to a true-stress, true-strain curve, the “uniform elongation” is no longer recognizable, and loses its meaning. Thus, reference to “uniform elongation” is meaningful only when a tensile test is being described. With this as background, we can now respond to the points raised in this item.

The proposed methodology is a total response analysis methodology based on a mechanistic formulation of the material's constitutive behavior within the finite element computational method. The computed strain response is a single quantity defined at individual points within the cladding thickness and along the length. It is possible to decompose the computed strain into its sub-component of elastic, plastic and creep, but it is not possible or meaningful to divide the computed strain into uniform elongation and total elongation. Thus, being a continuum based analysis method, one applies a continuum based failure criterion to the results to judge cladding integrity. Such a failure criterion is derivable from tensile tests and other rate dependent tests, but it cannot be a direct application of the uniform or total elongation measured in tensile tests. For example, the CSED is such a criterion that was derived from tensile and burst tests. This seems to be the fundamental difference between the EPRI methodology and the NRC staff's interpretation of cladding creep behavior.

True, the derivation of the circumferentially averaged 2% strain limit from the Garde et al. data is based on the total elongation, but it accounts only for strain rate effects, maintaining the stress to be in the plastic regime, which clearly is not a condition in dry storage. The fact that the cladding stress remains well below the yield strength, and the pressure is continuously decaying, justifies the use of a strain criterion derived from plastic flow consideration. However, as frequently mentioned in this document, the final criterion that will be proposed by EPRI will not be based on strain alone, as presented below. Therefore, the question of whether the 2% strain should be based on the uniform or total elongation loses significance.

With respect to the effect of potentially adverse localized cladding microstructural features (such as hydride lenses), the proposed methodology and criteria safeguard against the consequences of such local damage features. Under representative dry storage conditions, the storage temperature would be decaying from an initial value of about 350-400°C, and the nominal applied pressure is generally less than 20% of the yield pressure for full thickness cladding. Allowing for thickness loss and the presence of hydride lenses, local stress could rise initially to 30-40% of the yield stress. We note that the available creep data from French sources, Reference 63 in Report 1001207, and Bouffioux's presentation at the DOE/NRC/EPRI meeting at PNNL, Oct.2-3, 2000, for 4-cycle CWSR Zr-4 pressurized specimens under constant temperature of 400°C shows strains below 0.25% within the testing period of 1000 hours for the lower stress regime (20% of yield). For higher stresses (30% of yield), the creep strain is close to 0.8% within similar time period. Under actual dry storage conditions, the time decaying temperature and pressure could limit the circumferentially averaged strains to 2% over the storage life, although in the local region beneath the hydride lens the strain could rise to several percent. In such a situation, we must safeguard against any consequences by preventing the stress from evolving to a level where it can lead to creep rupture.

As an alternative to the circumferentially averaged 2% strain limit, a criterion will also be proposed in the third report, which will use the material's yield strength as the figure of merit.

***B-7. The last paragraph on page 5-1 states that, "This demonstrates that in the event of fracture, the crack will propagate slowly in a self-similar manner.....before it can extend axially in a burst mode. The above calculations are valid for all cladding conditions regardless of oxide thickness or the state of the oxide, coherent or spalled." Justify that the velocity of the pressure wave is greater than the velocity of the crack. Additionally, since there are limited data applicable to high burnup fuel under dry cask storage conditions, describe the uncertainties associated with both the selection of the pin-hole-equivalent mode of failure and the fracture toughness data that were used to perform the calculations.***



The issue being examined is whether a radially propagating crack to a through-wall configuration can extend axially dynamically to large length such as to threaten the containment of the fuel pellets or impair handling operation. In their review of the EPRI Report, PNNL drew a parallel between the gas pipeline problem and the fuel rod. PNNL's analysis is documented in Ref. 1 (Letter from Kimberly Gruss to Wayne Hodges, USNRC, July 3, 2001). We have re-analyzed the problem, and on the basis of our analysis, we concluded that: (a) a through-wall crack will depressurize before it can extend axially - the crack propagation velocity is  $1/10^{\text{th}}$  the gas pressure wave velocity; (b) a crack stability analysis shows that a through-wall crack is stable under the maximum fuel rod pressure, which negates the condition for dynamic instability; (c) PNNL's own analysis shows that the material has sufficient toughness for crack arrest, but to be conclusive they call for more analysis. Our analysis of the problem is documented in Attachment 1.

## **Section C: EPRI Report 1001281, "Fracture Toughness Data for Zirconium Alloys -- Application to Spent Fuel Cladding in Dry Storage," January 2001**

***C-1: The derived CSED values account for the sum of both crack initiation and crack propagation K values. However, the threshold fracture toughness (K) values for various mechanisms, such as DHC for example, utilize the threshold crack initiation values for K. Please justify the use of CSED-derived K-values for fracture mechanism considerations.***

The  $K_{IC}$ -CSED correlation, unlike the  $J_R$  curve, is not a crack resistance correlation, but a condition for unstable fracture. The discussion in response to items B-3 and B-4 gives further information.

***C-2. The submittal considers an approach relating a critical strain energy density (CSED) value for any material to the corresponding fracture toughness for the material. Essentially, the CSED is equated to the integrated stress-strain area in a mechanical strength test. The CSED values and associated estimated fracture toughness are then compared with fracture/rupture data. In the report, it is shown that the behavior of CSED as a function of cladding oxide thickness is different for the different loading (stress) conditions. However, in general, creep tests, tensile tests, and impact load-type (fracture toughness) tests involve different stress and temperature states and different fracture mechanisms. Show that the set of CSED data presented in the report is applicable for the range of stress and temperatures that are typical of dry cask storage. Although the potential complications are recognized in the paper, provide a detailed and complete CSED analysis relevant to Zircaloy clad fuel, including confirmation and verification of analysis with data from high-burnup fuel.***

The sentence, "In the report, it is shown that the behavior of CSED as a function of cladding oxide thickness is different for the different loading (stress) conditions." must be referring to Figure 3-4 in EPRI Report 1001207, which is reproduced below as Figure 1 for easy reference.

The critical strain energy density (CSED) is constructed from mechanical property tests using the integral,  $CSED = \int \sigma_{ij} d\epsilon_{ij}$ , where  $\sigma_{ij}$  and  $\epsilon_{ij}$  are the stresses and strains measured in the test. Repeated indices imply summation. As the integral implies, the definition of CSED admits uniaxial as well as multiaxial tests, which defines CSED as the total mechanical energy delivered to the material by the loading that contributed to failure. CSED has the units of energy per unit volume, i.e., MJ/m<sup>3</sup>, or MPa, and is by definition a normalized quantity. However, it is dependent on the environment and material conditions, such as temperature, hydrogen concentration, flaws and defects, etc. These factors, plus the usual experimental scatter contributed to the spread in the data in Figure 1.

With respect to the last sentence under C-2 RAI, the best information on the use of the CSED model in the analysis of high burnup fuel, which can be provided, is in predicting the behavior of the RIA tests conducted in France and Japan during the last several years. The information is familiar to the NRC, and a brief description is given in Reference 3. Figures 2 and 3, Yang et al. [3], show additional data than is contained in the above figure. These new figures show small changes in the best-fit curves, but no fundamental changes are introduced. Also the data is separated by temperature, where Figure 2, for the higher temperature, is the more applicable to spent fuel storage. It should be noted that we are not proposing a CSED-based criterion for spent fuel storage, although it may be worth investigating. We are, however, using the  $K_{IC}$ -CSED correlation to estimate the fracture toughness values for cladding

with spalled oxide and hydride lenses, shown in the CSED figures as solid symbols. The  $K_{IC}$  derived from the CSED was used to evaluate the effect of incipient cracks on DHC. In summary, we have:

- (a) The CSED is used to derive fracture toughness, but not to judge cladding integrity in dry storage, although its application as a dry storage criterion could be investigated.
- (b) The CSED data shown in the figures presented here constitute all presently available data.
- (c) The conservative nature of the  $K_{IC}$ -CSED correlation, together with the above information, should be adequate to base reasonable engineering judgments.

**Best Fit, Non-Spalled, and Spalled Data for  
CSED vs. Oxide/Cladding Thickness Ratio**  
Data from CC/ANO-2

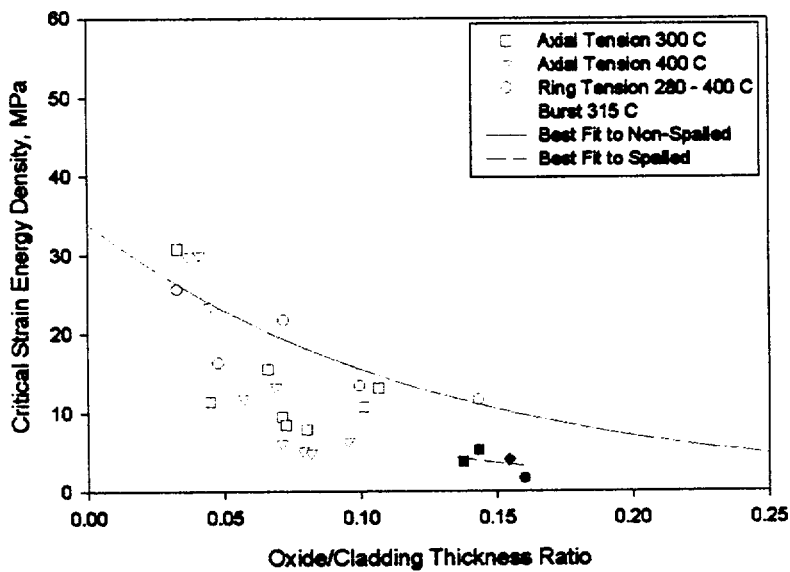


Figure 1 - Critical Strain Energy Density

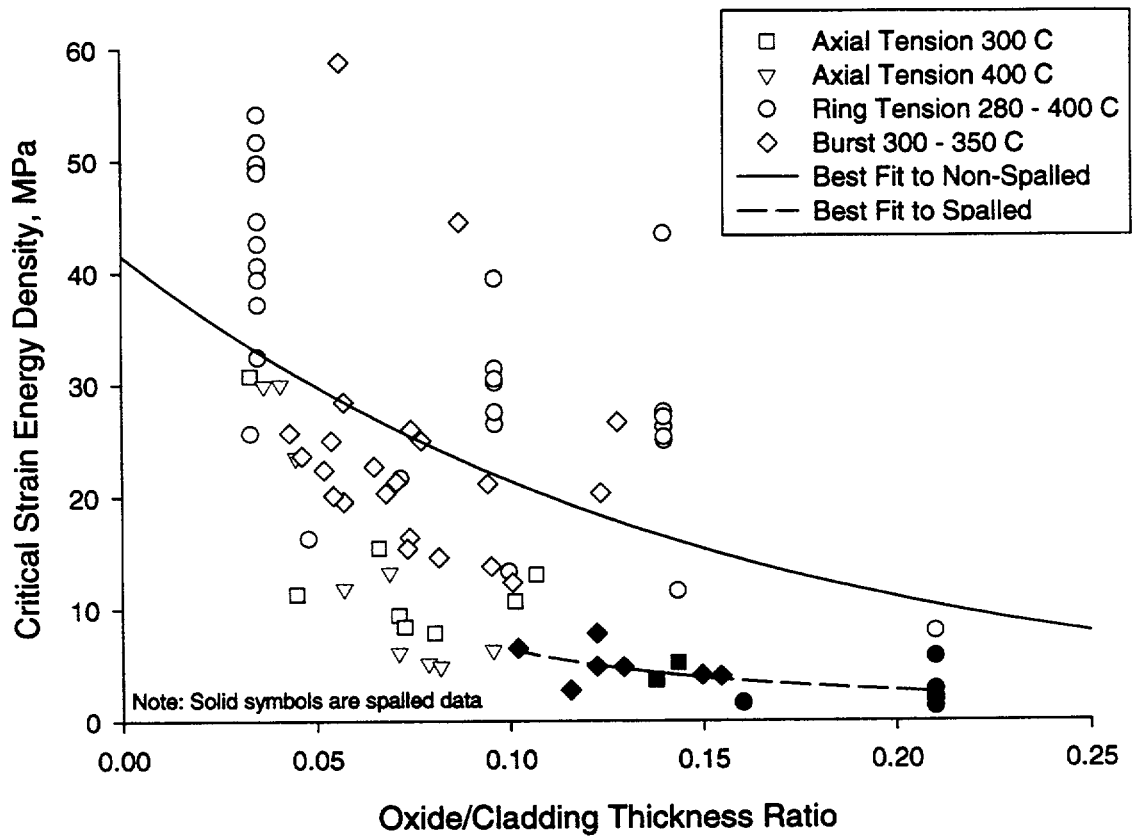


Figure 2 - Critical Strain Energy Values from Mechanical Property Tests at Temperatures Above 280°C

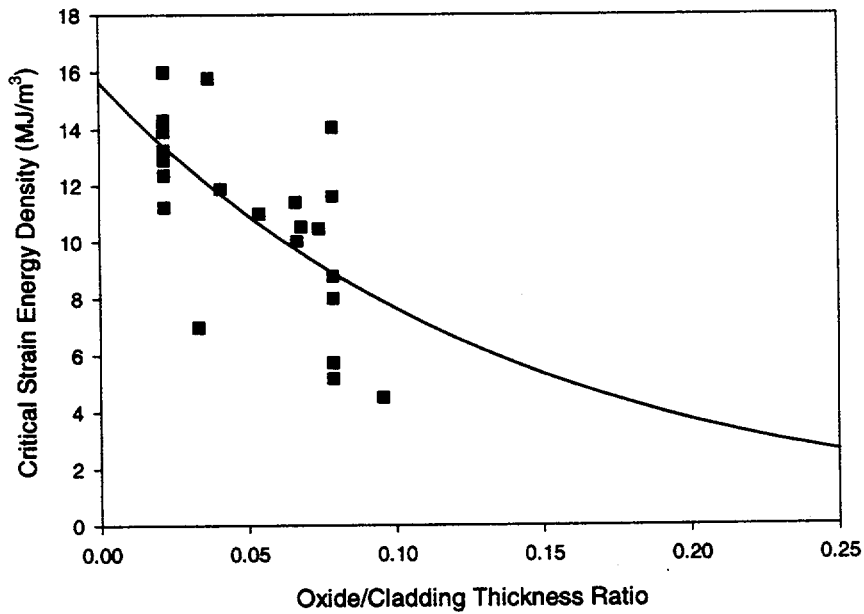


Figure 3 - Critical Strain Energy Values from Mechanical Property Tests at Temperatures Below 150°C

**C-3. Provide justification for the assumptions related to the assigned value for the critical plastic zone size and its influence on the ductility ratio, applicable to different materials. Although the applicability of the CSED methodology has been successfully demonstrated for aluminum, a similar demonstration of the applicability of this method for ferritic steels could not be reproduced. The report is not clear as to what strain should be used in the integration of stress-strain behavior, namely, strain based on elongation of gauge length, strain based on reduction in cross-sectional area, or an average of the two. Assuming that this plastic zone size (which is apparently considered a constant in the report) varies in the same manner as strength for different materials, provide supporting information on the variation of this plastic zone size for different zirconium-based materials under typical high-burnup conditions as a function of dry storage operating conditions.**

It should be noted at the outset that there is a misprint on page 5-3 of the report in the value of  $\rho_y = 10 \times 10^{-6}$  m. The correct expression is  $\rho_y / (2r-1) = 10 \times 10^{-6}$  m. This error may have been a source of confusion as evident by the statement, "Assuming that this plastic zone size (which is apparently considered a constant in the report)...". For that we apologize.

The size of the plastic zone enclosing the crack tip in specimens satisfying plane strain conditions is proportional to the quantity  $(K_{IC} / \sigma_{ys})^2$ . Rolfe and Barsom [4] gave the following expression for the radius of the plastic zone in a plane strain specimen,

$$\rho_y \cong \frac{1}{6\pi} (K_{IC} / \sigma_{ys})^2$$

This expression gives a value of about 40  $\mu\text{m}$  for the plastic zone radius for typical high burnup Zircaloy, as shown in EPRI Report 1001281. The above equation also affects the specimen thickness selection for satisfying plane strain requirement. Therefore, different specimen thickness will be required for high burnup Zircaloy than for ferritic steels or even unirradiated Zircaloy. But restricting our discussion to the material of interest, namely, high burnup Zircaloy, the EPRI report is self-consistent in its derivations.

**C-4. In paragraph 4 on page 2-2 of the report, it is not clear how the assumption that  $J_{IC}$  is the same for all fracture orientations is supportable. As an alternative to justifying this assumption, determine whether a prediction can be made regarding the most unfavorable orientation of applied stress-hydride orientation, and crack orientation with respect to the lowest fracture toughness value. This would then provide a conservative base value of fracture toughness for Zircaloy cladding.**

The question raised in the first sentence is a bit confusing. We are not making any assumptions on  $J_{IC}$ , the report simply describes the limitations on fracture toughness testing for cladding geometry, which is restricted to a through-wall planar crack extending axially. The reviewer is correct, however, in raising the issue of applying a fracture toughness derived for such a crack to, say, an incipient radial crack. Unfortunately, cladding geometry makes it impossible to evaluate a radial crack propagation experimentally. This is the reason for seeking help in the CSED correlation.

**C-5. In paragraph 3 on page 5-2, it is unclear how the second postulate is "suggested," based on the parameters  $\rho_y$  and  $r$  which play the same physical role in characterizing the level of ductility of the material. It is also unclear how that postulate led to deriving Eq. 11. Clarify the derivation and parameters in Eq. 12.**

Equation 11 is the second postulate; it is not obtained by derivation. The parameters  $\rho_y$  and  $r$  indeed play similar physical roles as is required, i.e., they both increase or decrease proportionately such that the ratio  $\rho_y / (2r-1)$  remains constant. This postulate is based purely on judgment. The Fracture Mechanics field is mostly an empirical science in which judgment has traditionally played a significant

role. With respect to Eq. 12, the typographical error discussed under Item C-3 may have led to the confusion. If the correct value is substituted, the equation checks out.

**C-6. Clarify the meaning of the symbol " $\sigma$ " in Eqs. 6 and 8. In the context of the prior discussion of Eq. 6,  $\sigma$  is the stress which is a function of the distance from the crack tip, whereas in Eq. 8,  $\sigma$  evidently has constant value. Further, justify the insertion of the expression " $\sigma^2/(2E)$ " in Eq. 8 which appears to be incorrect.**

An explanation following Eq. 8 is given, but it may not have been clear. The "pseudo-elastic" stress  $\sigma$  is the stress in the ideal LEFM material, see Figure 5-1 in the report. The right side of Eq. 8 is not derivable from the left side, but is a definition of the strain energy density in the real material at failure. The second = sign in this equation should have been a definition sign, namely,  $\equiv$ . Equation 8 simply equates the critical strain energy density in the idealized LEFM material to the real material.

**C-7. Correct the sentence as it appears prior to Eq. 10. It appears that this sentence should read, "....substituting Eq. 9 in Eq. 7...."**

Thank you.

**C-8. In the last paragraph on page 5-2, for a typical high burnup cladding material, a value of 40  $\mu\text{m}$  has been calculated using a  $K_{IC}$  estimate of 20  $\text{MPa}\sqrt{\text{m}}$  and a yield strength of 700 MPa. However, using Eq. 7 in the paper, one can obtain a value of approximately 130  $\mu\text{m}$ . Justify whether a value other than  $(1/\sqrt{r\pi})$  has been used for the shape factor ( $Y$ ) in the fracture mechanics equation.**

Equation 7 applies to plane stress, whereas the numerical value for  $\rho_y$  is for plane strain, see response to C-3 above. The intent was to derive a correlation that uses the strain energy density, which is independent of plane strain and plane stress conditions. The two parameters  $\rho_y$  and ductility ratio  $r$ , combined in the ratio  $\rho_y/(2r-1) = 10\mu\text{m}$ . This ratio is postulated (second postulate) to remain constant. This should have been clarified better in the report.

**C-9. In the last paragraph of page 6-2, an internal gas pressure of 7.5 MPa has been assumed under reactor operating conditions. From this stress, a stress intensity factor of 2  $\text{MPa}\sqrt{\text{m}}$  is calculated for a crack that extends through 40% of the cladding thickness. The value of 2  $\text{MPa}\sqrt{\text{m}}$  is below the threshold stress intensity factor of 5-6  $\text{MPa}\sqrt{\text{m}}$ , which is required for Stage 1 of the delayed hydride cracking (DHC) process. However, the EPRI creep report indicates that the cladding hoop stress, under spent fuel dry storage conditions, is less than 150 MPa. Since the stress intensity factor is proportional to stress, it is not clear that the stress intensity factor, under the assumed crack size and geometry would stay within the threshold stress intensity factor for DHC. Clarify the justifications for this conclusion.**

The referenced paragraph gives two examples, a BWR and a PWR. The above value of 2  $\text{MPa}\sqrt{\text{m}}$  is for a BWR, but the value for PWR under the same assumptions is calculated to be 5  $\text{MPa}\sqrt{\text{m}}$ . The calculations seem to be consistent, but the text apparently was not sufficiently clear.

**C-10. In paragraph 4 on page 3-1, clarify the meaning of the following sentence, "Despite the differences in the microstructure from the first material set, the fracture toughness values are similar for a similar range of conditions." A contradiction to this statement exists on page 4-1, paragraph 1, which says that values may be different for beta-quenched material. Additionally, page A-2 containing the tabulated data also reiterates that the "microstructure is not typical of modern cladding materials." This statement implies that the microstructure of the material used to obtain the data imparts some difference on the data. Further, justify why cladding microstructural characteristics (e.g., precipitate type, form, and morphology, annealing parameter, or texture) do not influence the fracture toughness parameters.**

We are simply reporting on the data as described by the authors. As further clarification, the sentence should have been written to read as follows, "*Despite the differences in the microstructure from the first material set, the fracture toughness values seem to be similar for a similar range of test conditions*". With respect to the last sentence in C-10, the report makes no statement that requires justification regarding the effects of microstructure on fracture toughness. In fact, by drawing attention to the difference in microstructure between the beta-quenched and alpha annealed materials, we are underlining the influence of microstructure on fracture toughness.

**C-11.** *In the last paragraph on page 5-2, the value of the parameter  $\rho_r$  is described as being "of the order of 10 microns." However, on page 5-1,  $\rho_r$  is described as a position corresponding to  $\sigma_r$ . Clarify the meaning and significance of this parameter  $\rho_r$ .*

Clarification is given under item C-3.

**C-12.** *In the first paragraph on page 6-1, the report makes reference to a paper that describes the delayed hydride cracking mechanism in CANDU pressure tubes. Please provide a copy of the relevant sections of Ref. 19, Proceedings of an International Symposium on Absorbed Specific Energy and/or Strain Energy Density Criterion, Sept. 17-19, 1980, G.C. Sih, E. Czoboly, F. Gillemont, Editors, Martinus Nijhoff Publishers, The Hague/Boston/London.*

The proper reference is 20 not 19. This is regrettably a typographical error.

**C-13.** *On page 4-1, a  $K_{IC}$  value of 12 MPa $\sqrt{m}$  is identified as a suggested value for material with hydrogen concentrations greater than 1000 ppm independent of temperature. Provide further justification for this conclusion considering the following comment. In the abstract, the report states that one of the objectives is to address applicable regulations and regulatory guidance for the storage of spent fuel. As such, one of the concerns is the issue of retrievability of the fuel after storage for further processing, transportation, and disposition of the spent fuel. Please evaluate the implications of the sensitivity and uncertainty in such fracture toughness analysis with respect to potential retrievability issues.*

Fracture toughness could play a useful role in judging cladding integrity under handling loads during retrieval operations. The 12 MPa $\sqrt{m}$  fracture toughness value is based on data, but it may be as low as 7.8 MPa $\sqrt{m}$ , or as high as 15-20 MPa $\sqrt{m}$ , depending on actual cladding conditions. The lower value was derived from the  $K_{IC}$ -CSED correlation for cladding with spalled oxide, and the higher value is a more typical value for high burnup cladding. It should be mentioned, however, that retrievability issues are addressed in Item A-1. There, we argued that, as long as creep rupture is prevented, handling loads during retrieval operations do not pose worse challenges to the fuel assemblies than before placement in dry storage casks.

## Section D: NEI Slides from the April 18<sup>th</sup> NEI/NRC Meeting

*D-1. The FALCON code was used to predict the creep behavior of Zircaloy cladding (slide 11). In those slides, good prediction was indicated for creep to rupture for only two creep specimens that appear to be from unirradiated cladding. Provide additional justification of the ability of the FALCON code to predict the creep behavior of a wide range of cladding materials and condition.*

The requested information will be provided in two parts. The first part is described in Attachment 3 to this document. The second part is contained in the Creep Methodology report, which is the third report in the series.

*D-2 Provide the models and assumptions used in the development of the FALCON code and describe how these models and assumptions are applicable to analyzing creep behavior of high burnup fuel under dry storage conditions. The models should be described in sufficient detail (with coefficients) to enable the NRC to replicate predictions of creep and creep to rupture.*

The Falcon code is the high-burnup version of the FREY code. The thermo-mechanics formulation of FALCON is identical to that in FREY. The documentation of FALCON is still being prepared, and will not be ready for some time. However, since the essential theoretical and numerical bases that affect creep analysis is the same in both codes, FREY's documentation should suffice for the present. The Theory Report and the Design Review Report for the FREY code are enclosed for evaluation.

### References

1. Letter, Kimberly Gruss to Wayne Hodges, Attachment 2, USNRC , July 3, 2001.
2. Ells, C. E., "Hydride Precipitates in Zirconium Alloys" (A Review), *JNM* 28 (1968), 120-151.
3. Yang, R. L., et al., "Industry Strategy and Assessment of Existing RIA Data", Proceedings of the International Topical Meeting on LWR Fuel Performance, Park City, Utah, April 10-15, 2000.
4. Rolfe, S. T., and Barsom, J. M., "Fracture and Fatigue Control in Structures", Prentice-Hall, Inc.



# Attachment 1

---

## Pin-Hole Failure Evaluation

### 1. Introduction

Reference 1 cited burst tests by Fuketa et al. on hydrided, high burnup cladding that exhibited narrow axial cracks from stable crack initiation and extension, as opposed to ductile tearing associated with typical burst testing. A plane-strain linear elastic fracture mechanics (LEFM) crack initiation fracture toughness value of  $K_{IC} = 7.8 \text{ MPa}\sqrt{\text{m}}$  was then used to estimate the critical crack driving force for an axial flaw extending  $600 \mu\text{m}$  through the cladding thickness. The critical crack driving force was found to be a cladding pressure (hoop) stress of 170 MPa, well above the maximum actual circumferential stress in the cladding thickness. The calculation was cited as the basis for cladding leakage before cladding burst.

The NRC staff review questioned the validity of the analysis, asking for information on depressurization rate versus crack propagation rate following initiation. The implication from the question is that the NRC staff:

- Accepts the principle that the nominal cladding stress is too low to cause crack initiation; but
- Because the cladding material in the high burnup (irradiated, hydrided) condition is relatively brittle;
- Does not accept that, for pressure loading sufficient to extend the crack axially or radially, some portion of the resulting crack extension is stable.

Therefore, the crucial concern is whether crack growth in the axial and radial direction can be shown to be stable prior to reaching the critical crack size for unstable propagation. This question is addressed in Section 2 below. This is followed by an evaluation of the potential for dynamic crack propagation in Section 3. Section 4 gives comments on PNNL's fracture mechanics calculations.

### 2. Crack Instability Calculations

A fracture mechanics analysis is performed to determine if it can be shown that crack growth under increasing load can remain stable prior to reaching the critical crack size for unstable propagation. Affirmative results mean that it would be impossible for constant or decaying internal pressure to drive the crack to unstable propagation.

The analysis relies on a realistic, but conservative, representation of toughness variation through the thickness to reflect the hydrogen radial profile. The fracture toughness through-thickness variations, as function of the local hydrogen concentration, are consistent with the data reported in EPRI 1001281, varying from 30 MPa√m at the inner surface to 6-7 MPa√m at the metal-oxide interface. The distribution of hydrides through the cladding thickness varies from 2000 ppm at the oxide-metal interface near the outer cladding surface to 200 ppm at the cladding inside surface. It is noted that the exact value of hydrogen concentration on the oxide metal interface is not important since minimum fracture toughness is used for the outer 25% of the cladding thickness. The hydrogen profile, and consequently the fracture toughness profile, used in the calculations reflect cladding conditions outside a hydride lens. This is justified on the basis that hydride lenses are quite localized

In the following calculations, the Zircaloy-4 cladding diameter will be chosen to be 10.92 mm (0.430 inches), with a cladding thickness of 0.635 mm. The ratio of the mean radius to the thickness is then 8.1. At 75 μm from the outside surface, at approximately the oxide-metal interface, the hydride concentration will be assumed to be 2000 ppm. The radius of this point is slightly less than 90 % of the way across the nominal thickness. At 165 μm from the outside surface (75 % across the wall thickness), the hydride concentration will be assumed to be 1000 ppm. At 365 μm from the outside surface (about 42 % across the wall thickness), the hydride concentration will be assumed to be 300 ppm, and will be assumed to be less than this value at positions nearer the cladding inner surface.

Therefore, for this hydride concentration profile, a reasonable and conservative set of assumptions for estimating crack growth stability would be to:

- Use elastic-plastic crack growth resistance data for evaluating axial and radial crack extension at points at or near the inside cladding surface, with an estimated fracture toughness of 30 MPa√m (27 ksi√in) at points from 0 to 20% of the inside surface of the cladding;
- Assume that the fracture toughness is reduced to 25 MPa√m (23 ksi√in) at a point 25 % of the distance from the cladding inside surface across the wall thickness;
- Assume that the fracture toughness is reduced to about 20 MPa√m (18 ksi√in) at a point 50 % of the distance from the cladding inside surface across the wall; and
- Assume that the fracture toughness is reduced to 6 to 7 MPa√m (5.5 to 6.4 ksi√in) at a point 80 % of the distance from the cladding inside surface across the wall.

Points intermediate to these points will be based upon interpolation, as required.

A flaw oriented in the axial/radial plane is postulated. As a starting point, the flaw will be assumed to extend from the inside diameter of the cladding to a depth,  $a$ , that is 20 % of the cladding thickness. This would imply a flaw depth of 127 μm. The flaw aspect ratio,  $a/c$  (flaw depth to flaw half length), will be assumed to be 0.2 ( $2c$  = flaw length = 1270 μm). Applied stress intensity factor solutions can be found in References 2 and 3. The circumferential tensile pressure-caused stress that drives flaw initiation and growth

will be assumed to be uniform across the cladding thickness, for conservatism. This stress will be unrealistically increased in order to determine the critical driving stress for the postulated flaw. That critical stress will be determined for both axial flaw extension (the c-tip of the flaw is critical) and for radial flaw extension (the a-tip of the flaw is critical). It should be noted that the material fracture toughness at the c-tip of the flaw is always the inside cladding surface fracture toughness, while the material fracture toughness at the a-tip of the flaw will decrease as the flaw extends radially.

For  $a/t = 0.2$ , the c-tip stress intensity factor from Reference 2 is 0.6110 and the a-tip stress intensity factor is 1.1445 (single-edge cracked plate), which implies a critical internal pressure of 320 MPa for the c-tip and 130 MPa for the a-tip. For this condition, if the internal pressure is increased well beyond the assumed maximum internal pressure of 21 MPa, the a-tip will control and the flaw will extend in the radial direction. However, this implies an increase in internal pressure of more than six times the maximum value. The 21 MPa for maximum pressure is equivalent to a critical stress of 170 MPa determined in EPRI Report 1001207 using a uniform fracture toughness of 7.8 MPa  $\sqrt{\text{m}}$ . Critical pressure is defined to be the pressure that produces a stress intensity factor equal to the fracture toughness. Critical stress is the far field stress caused by the critical pressure.

For  $a/t = 0.5$ , the c-tip stress intensity factor is 0.7802 and the a-tip stress intensity factor is 1.4504, which implies a critical internal pressure of 315 MPa for the c-tip and 85 MPa for the a-tip. For this condition, the internal pressure would have to increase by a factor of 4 over the nominal internal pressure for the a-tip to of the flaw to initiate. The c-tip is again extremely far removed from initiation and does not control.

The complete range of calculations for the c-tip and a-tip of the postulated flaw, as a function of the dimensionless flaw depth,  $a/t$ , is shown in Figure 1. Note that the flaw depth must increase to  $a/t = 0.75$  before internal pressure can cause flaw initiation at the a-tip. For that same flaw, the internal pressure necessary to cause the flaw to extend axially is 125 MPa, 6 times the maximum internal pressure.

The critical flaw depth at which internal pressure can cause radial flaw extension is about  $a/t = 0.75$ , or a flaw depth of about 0.54 mm. At such a flaw depth, unstable flaw extension through the remainder of the cladding thickness will be caused by an internal pressure of 21 MPa. For that same flaw depth, the circumferential stress is too low, by a factor of 6, to cause axial flaw extension. However, if such a stress were possible, the flaw extension would be stable, as the results of crack growth resistance in the elastic-plastic region.

## 2.1 Conclusions

The margin against axial flaw instability is very large. This margin would, under actual spent fuel conditions, substantially and rapidly increase as a result of the local depressurization that would occur at through-wall crack occurrence. The large margin shown in Figure 1 against unstable axial crack propagation leaves substantial room for using even lower fracture toughness values in the calculations without changing the outcome.

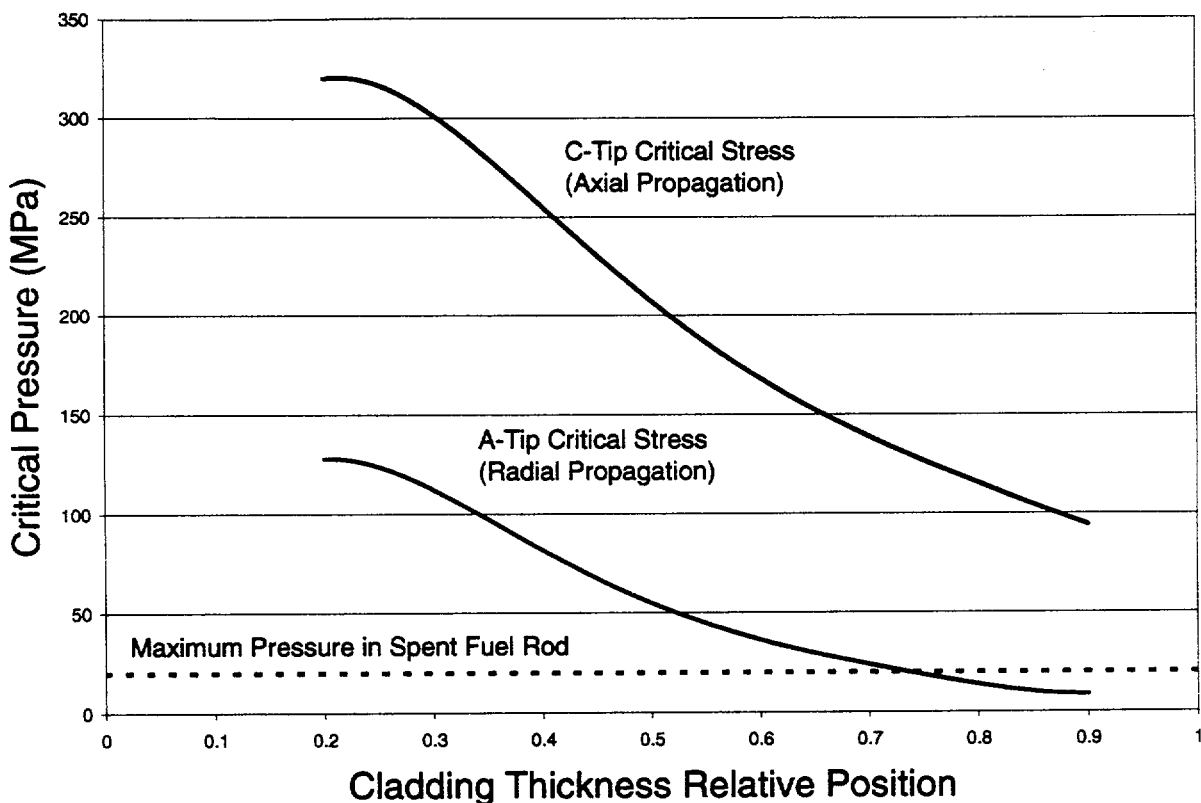


Figure 1 – Crack Stability Profile

### 3. Evaluation of Conditions for Dynamic Crack Propagation

The crack stability calculations described in the preceding section show a very large margin against axial flaw instability. These calculations support the EPRI Report 1001207 thesis that a cladding failure under dry storage conditions, regardless of whether or not it can occur, is equivalent to a pinhole. However, historical data for gas pipeline rupture was quoted in Reference 4 as an example where dynamic crack propagation can occur in a pressurized tube, with the implication that similar failure could occur in fuel rods in dry storage, and should be investigated. The gas pipeline rupture attracted great deal of analytical and experimental work, (see cited references in References 5 and 6). The figure of merit used to assess the potential for dynamic failure in spent fuel rods is the ratio of the depressurization velocity to the limiting crack velocity. This ratio must be shown to be greater than unity for dynamic crack propagation not to occur.

The problem of dynamic crack propagation in a fast reactor fuel pin was studied by I. J. Ford at Harwell Laboratory [5,6], as part of accident evaluation of the consequences of fuel melting. Ford compared his analysis to Freund and Parks [7], and validated his model against several British and US tests, with measured and calculated crack velocities

in the range of 125 to 260 m/s. Studying Ford's analysis of a stainless steel fast reactor fuel pin, we determined that Ford's model is directly applicable, upon substitution of the appropriate material properties, to a PWR fuel rod. Ford gave the following expression for the crack velocity [6],

$$v^2 = \frac{8a^2}{\rho_c \delta h \pi^2} \left[ p - \frac{\pi \sigma_y h^2}{a^2} - \frac{\sigma_y h^2}{4r^2} + \left( \sigma_\theta^2 - \frac{K^2}{\pi r} \right) \frac{h}{E \delta} \right] \quad (1)$$

where,

$$\delta = 2r^2 \varepsilon_\theta / h, \quad (2)$$

and

$$a^2 = \alpha r h \quad (3)$$

For conservatism, we neglect the plastic energy dissipation terms in Eq. 1. This reduces Eq. 1 to,

$$v^2 = \frac{8a^2}{\rho_c \delta h \pi^2} \left[ p + \left( \sigma_\theta^2 - \frac{K^2}{\pi r} \right) \frac{h}{E \delta} \right] \quad (4)$$

To maximize the velocity, we minimize  $\delta$  by setting the hoop strain  $\varepsilon_\theta$  equal to the elastic strain under a stress of 150 MPa. Eq. 4 is evaluated using the following parameter values:

$v$  : Crack Velocity (m)

$\alpha$ : A constant assigned the value of 14

$r$  : Radius of the cladding tube 4.5 mm = 4.5E-3m

$h$  : Cladding thickness = 0.5 mm (excludes metal loss) = 0.5E-3m

$a$  : Length of the crack tip region, calculated from Eq.3, = 5.6125E-3 m

$\rho_c$ : Density of the cladding material = 6500 kg/m<sup>3</sup>

$\sigma_\theta$ : Cladding hoop Stress = 150 MPa

$E$ : Elastic Modulus = 96,000 MPa

$\varepsilon_\theta$ : Cladding hoop Strain =  $\sigma_\theta / E = 150/96,000 = 1.56E-3$

$\delta$  : Maximum radial displacement, calculated from Eq. 2, = 4.05 E-5 m

$p$  : Pressure = 16.67 MPa

$\sigma_y$ : Yield stress of the cladding material, not used

$K$ : Fracture toughness of the cladding = 8 MPa√m

The crack velocity is calculated to be 36 m/s. From Reference 4, the sonic velocity was estimated to be 411 m/s. The ratio of the depressurization velocity to the limiting crack velocity is greater than 10, with equal margin against the formation of long axial cracks.

#### 4. Comments on PNNL's Analysis

As can be seen, the above results are quite different from the PNNL analysis described in Reference 4. One possible explanation is that the analysis of Reference 4 is an extrapolation whereas the present results are a direct application of an analysis developed for fuel rod geometry. This extrapolation deals only with geometry and material properties effects, ignoring the amount of stored energy in the pressurization medium. The stored energy is the pressure times volume, and for equal pressure the stored energy per unit length is proportional to the volume. Simple calculations would show that the stored energy ratio of gas pipe to fuel rod is in the range of 600 to 3000, depending upon whether we consider the total fuel rod gas volume or just the fuel-cladding gap.

PNNL first showed that the ratio of the depressurization velocity to the limiting crack velocity is less than unity, implying unstable dynamic fracture. Then, a fracture mechanics calculations was used to determine the minimum fracture toughness needed to arrest a crack in a steel pipe with the same dimensions as a fuel rod. This minimum toughness was determined to be about  $3.3 \text{ MPa}\sqrt{\text{m}}$ , which is not much larger than that of a pure hydride ( $1-3 \text{ MPa}\sqrt{\text{m}}$ ). This is a factor of 2 smaller than the minimum fracture toughness value of  $7.4 \text{ MPa}\sqrt{\text{m}}$  measured by Kreyns et al. for 4000-ppm hydrogen charged test specimen. However, despite such margin, the results were dismissed because the fracture toughness value came from hydrogen-charged material, arguing that non-uniformly hydrided specimens may have lower ductility. The conclusions were that the results were not sufficient to form an opinion and called for more studies.

A second set of calculations was performed to account for through-thickness variation of fracture toughness, with the minimum value of fracture toughness assigned to the inner 50% of the thickness and zero to the outer 50%. The following assumptions were made: (a) Hydride rim 50% of clad thickness extending the entire length of the rod, (b) Totally fractured hydride rim, reducing the effective cladding thickness to 50% of thickness remaining after corrosion, (c) 275 MPa stress in the cladding over the entire length, (d) Axial through-wall cracks ranging from 0.1 to 0.4 inch simulating the axial extent of a hydride lens. The calculations show that the stress intensity factors, even for the shortest crack, exceeded the fracture toughness of  $7.4 \text{ MPa}\sqrt{\text{m}}$  by a significant margin.

The following comments come immediately to mind:

- (a) Typical hydride rim thickness in high burnup cladding is of the order of  $50 \mu\text{m}$ , and is a relatively tough material: low toughness, but not zero as assumed. Note that the fracture toughness of a solid hydride is  $1-3 \text{ MPa}\sqrt{\text{m}}$ .
- (b) The assumed hydride rim geometry and properties are equivalent to a solid hydride occupying the outer half of the cladding along its entire length. The maximum penetration of a hydride lens can be as much as 50% of cladding thickness, but is limited in the axial direction to a few clad thicknesses and to about 15-30 degrees circumferentially. Therefore, even if we assume the local stress (in the ligament beneath the hydride lens) of 275 MPa governs the crack extension locally, it eventually runs into more ductile material, with lower stress and higher toughness.

Under the highly conservative assumption of hydride lenses lining up in the same axial plane, a much higher (than the  $7.4\text{MPa}\sqrt{\text{m}}$  value used) fracture toughness of the material between the hydride lenses governs the axial propagation of the crack.

- (c) A more realistic calculations, would start with a short through-wall crack that simulates a fully cracked hydride lens/ligament, calculate the stress intensity factor for the tube geometry and then compare it to the fracture toughness of the material outside the hydride lens. Such calculations were actually made about six years ago in connection with the secondary failures of BWR barrier cladding, see Reference 7. The calculations were three-dimensional in which the J-Integral was computed and  $K_I$  then calculated assuming elastic fracture. The following expression was derived for the stress intensity factor:

$$K_I = \beta * (1 - e^{-4.7x}) * \sigma \quad (1)$$

Where  $\sigma$  is the intact hoop stress,  $x$  is the crack length in inches, and  $\beta$  is the Pellet-Cladding Mechanical Interaction Coefficient having the values 0.86 and 2.15 for slip and stick conditions, respectively. Using  $\sigma = 40$  ksi,  $\beta = 0.86$ , which applies to the pressurized tube case, we calculate stress intensity factors of 12.9, 21.0, and 29.2 ksi $\sqrt{\text{in}}$  for the 0.1, 0.2 and 0.4 inch cracks, respectively, instead of the 26.2, 53.8 and 104.6 ksi $\sqrt{\text{in}}$  given in the PNNL calculations, which are factor of 2 to 3.5 higher. We note that the minimum fracture toughness used in the DEFECT code is 15ksi $\sqrt{\text{in}}$ , which gave validated predictions of axial cracking in BWRs. A fracture toughness value of 15ksi $\sqrt{\text{in}}$  for the cladding material outside the hydride lens would arrest the crack.

## 5. Summary and Conclusions

- (a) Crack stability analysis based on realistic assumptions for the fracture toughness through-thickness profile shows a large margin against unstable axial crack propagation.
- (b) Using a dynamic crack propagation analysis specific to fuel rod geometry, the ratio of depressurization wave velocity to crack propagation velocity is at least 10.
- (c) Adopting more realistic assumptions in PNNL's analysis, it can be shown that a through-wall axial crack remains sub-critical.

## 6. References

1. Chapter 5, "Pin-Hole-Equivalent Failure Mode," Untitled EPRI Report submitted to the NRC Staff for review.
2. Raju, I. S., Mettu, S. R., and Shivakumar, V., "Stress Intensity Factor Solutions for Surface Cracks in Flat Plates Subjected to Nonuniform Stresses," *Fracture Mechanics: Twenty-Fourth Symposium, ASTM STP 1207*, J. D. Landes, D.

- E. McCabe, and J. A. M. Boulet, Editors, American Society for Testing and Materials, Philadelphia, PA, 1994, pp. 560-580.
3. Buchalet, C. B. and Bamford, W. H., "Stress Intensity Factor Solutions for Continuous Surface Flaws in Reactor Pressure Vessels," *Mechanics of Crack Growth, ASTM STP 590*, American Society for Testing and Materials, Philadelphia, PA, 1976, pp. 385-402.
  4. Letter, Kimberly Gruss to Wayne Hodges, Attachment 2, USNRC , July 3, 2001.
  5. Ford, I. J., Axial Crack Propagation in Fuel Pin Cladding Tubes, *Nuclear Engineering and Design*, 136 (1992) 243-254.
  6. Ford, I.J., "Rupture and Fragmentation of Pressurized Pipes and Fast Reactor Fuel Pins", *Trans. of the 12<sup>th</sup> Int. Conf. On Structural Mechanics in Reactor Technology, Vol. C*, MPA, University of Stuttgart, August 15-20 1993.
  7. Freund, L. B. and Parks, D. M. "Analytical Interpretation of Running Ductile Fracture Experiments in Gas-Pressurized Linepipe", ASTM STP 711, p. 359, 1980.
  8. DEFECT – Defective Fuel Element Code-T, Volume 1: Theoretical and Numerical Bases, EPRI TR-107887-V1, August, 1997.



## Attachment 2

### CREEP AS THE GOVERNING MECHANISM OF SPENT FUEL IN DRY STORAGE

**Joseph Y. R. Rashid**  
ANATECH Corp.  
5435 Oberlin Drive  
San Diego, California 92121  
USA

**Albert J. Machiels**  
Electric Power Research Institute  
3412 Hillview Avenue  
Palo Alto, California 94304  
USA

#### ABSTRACT

Potential damage mechanisms postulated for spent fuel in dry storage include stress corrosion cracking (SCC), delayed hydride cracking (DHC), and accelerated (tertiary) creep leading to creep rupture. The primary conditions that govern the evolution of these damage mechanisms during dry storage are the spent fuel rod's internal chemical environment and its thermal and mechanical histories. In a recent publication, (see cited references), thorough evaluation of these mechanisms, utilizing conservative estimates of pre-existing thermomechanical and physical conditions of the cladding, show that SCC and DHC are not likely operative mechanisms in dry storage. This leaves creep rupture as the primary mechanism of concern. Evaluation of this mechanism is the subject of the present paper. Results of creep modeling and analysis are presented to show that self-limiting creep deformations govern the behavior of fuel rods in dry storage. This leads us to suggest that a liberal strain limit of several percent, with a side condition on stress evolution to remain below the local yield strength, is an appropriate acceptance criterion for dry storage.

#### INTRODUCTION

Licensing regulations for spent fuel dry storage in the United States divide the fuel into two groups: low-to-medium and high burnup, with assembly-average burnup of 45 GWd/MTU as the dividing line. Operational criteria in terms of short-term and long-term temperature limits are used as the licensing basis for the first group. In contrast, physical limits are specified for the higher burnup fuel, including setting specific limits on oxide thickness, e.g., 80  $\mu\text{m}$ , and creep strain, e.g., 1%, as the means to ensure cladding integrity during storage. Arguments in support of these limits rely on tube tensile and burst data by Garde et al. [1] and Fuketa et al. [2] for high burnup cladding with spalled oxide. However, in a recent ICONE9 paper [3], based on an EPRI report submitted to the USNRC in support of an industry position on spent fuel dry storage [4], a detailed analysis of this data supports an acceptance criterion of at least 2% strain. Moreover, given that creep rupture is a manifestation of plastic instability, which is a condition of the material's ultimate tensile strength, strain alone is not sufficient to define the onset of plastic instability under creep. Consequently, a fully prescribed criterion requires that both the stress and the strain be defined. The evolution of the hoop stress with time as a result of creep-induced wall thinning uniquely determines whether a state of plastic instability can result from creep deformations initiated at stress levels typical of spent fuel rods in dry storage.

Cladding creep response during dry storage depends on many material-dependent and operation-dependent factors. The former define the fuel rods dry storage initial conditions such as cladding type, residual cold work, effective fast fluence, outer-surface oxide thickness and coherence, hydrogen concentration, hydride levels, and cladding defects. Operation-dependent conditions consist mainly of the

fuel-rod temperature and pressure time-histories during dry storage. Both of these sets of conditions are incorporated into a creep-based methodology, as will be described in this paper. An outline of this methodology is given below.

Part 1 – Dry Cask Storage System (DCSS) Thermal Analysis:

1. Decay heat model as a function of burnup, initial enrichment, and cooling time
2. Heat transfer models to calculate peak rod temperature and peak cladding temperature

Part 2 – Fuel Rod Creep Analysis:

1. Fuel rod parameters (initial helium backfill and fission gas release, rod free volume, initial cladding thickness, cladding wastage)
2. Cladding creep model and creep data describing post-irradiation creep response and failure potential as functions of cladding type, temperature and stress.
3. A fuel rod behavior code that integrates the above models and data into a response analysis procedure.

The thermal analysis of the dry cask storage system (DCSS) in Part 1 is accomplished using well-known source-term computer codes, e.g., ORIGIN2, and DCSS-dependent heat transfer calculations. These calculations define the initial temperature and in-storage thermal history of the cladding, which become the input to the creep analysis process in Part 2. This paper deals with Part 2 only, but in order for the creep calculations to proceed, a simulation of Part 1 calculations is used, as will be described in the paper.

## POST-IRRADIATION THERMAL CREEP MODELS

Despite the extensive work that has been done during the last four decades in the area of in-reactor creep modeling, Franklin et al. [5], limited information is directly transferable to post-irradiation creep. In the majority of cases, the thermal creep sub-models in fuel performance codes are integrally dependent on their host codes, both in numerical structure and experimental validation, and cannot be easily separated from those codes to allow their use in out-of-pile creep analysis. Therefore, one must effectively begin anew, choose a suitable mathematical form for the model, and then quantify the model parameters from new test data. A general form of a phenomenological creep-rate law can be expressed as follows,

$$\dot{\epsilon}_{p,s}^c = f_{1p,s}(\sigma) * f_{2p,s}(T) * f_{3p,s}(\epsilon_p^c) * A_{p,s}(\psi) \quad (1)$$

The subscripts  $p$  and  $s$  stand for primary creep and secondary creep respectively. The total creep rate is obtained by adding the individual primary and secondary terms. Equation (1) is a form of strain-hardening law in which the cumulative primary creep strain  $\epsilon^c$  replaces time as an independent variable. The secondary creep rate is by definition independent of time, which makes  $f_3$  identically unity. The parameter  $A(\psi)$  contains the effects of prior irradiation hardening and is written as a function of fast fluence  $\psi$ . Equation (1) serves as a generalized template for the thermal creep models currently considered for spent fuel creep analysis.

### Spent-Fuel-Specific Models

The development of creep models for application to spent fuel in dry storage with the attributes shown in Eq. (1) is mainly due to French researchers at CEA and EDF. These models will be the primary tools for the creep-based methodology described in this report.

**CEA-EDF Model-1:** This model, developed by Limon et al. [6], was derived for creep data obtained for Cold Worked Stress Relieved (CWSR) cladding from FRAMATOME 4-cycle rods with burnup level of approximately 47200 MWd/MtU. The stress is in the range of 150-250 MPa, and the temperature is in the range of 380-420°C. The longest duration of the creep tests is roughly 1350 hours. The model is formulated as a primary-creep-only model.

Casting the CEA-EDF Model-1 in the form of Eq. (1) leads to the following expressions.

$$f_{1p}(\sigma) = V_0 * \sinh\left(\frac{\sigma_{\theta\theta} - \sigma_{rr}}{\sigma_c}\right) \quad (2)$$

$$f_{2p}(T) = \exp(-T_a / T) \quad (3)$$

$$f_{3p}(\varepsilon) = (\varepsilon_{\theta\theta} + \varepsilon_0)^{-p} \quad (4)$$

$$A \equiv 1 \quad (5)$$

where

$$p = 0.9, \varepsilon_0 = 0.000045, V_0 = 3.47 \times 10^7 s^{-1}, \sigma_c = 34 MPa, T_a = 32000 K \quad (6)$$

The influence of 4-cycle irradiation hardening on the creep rate is implicitly included in the model constants shown above, thereby restricting the model's use to fuel rods with this particular level of irradiation. Also, because of the absence of an explicit secondary-creep term, the model's application to long-term storage could limit its use. As we shall see, however, creep deformations saturate relatively early, and the extrapolation of short-term data may be fully justifiable.

**CEA-EDF Model-2 and Model-3:** These models are closely related and are discussed together. Model-2 appeared in an EDF internal report by Jean-Marie Gras [7]; Model-3, which is the subject of a paper in the present ICM01 conference, was made available to EPRI through private communication with Pol Bouffieux [8]. Both models include primary and secondary creep terms with explicit dependence of both terms on fast fluence. By including fast fluence explicitly, the models conveniently extrapolate un-irradiated creep data to any irradiation level. The changes from Model-2 to Model-3 involve new values for the model constants and the introduction of linear fluence term for the secondary creep component, in place of the Model-2 exponential dependence; however, the exponential dependence was retained for the primary creep term. Model-2 and Model-3 have the same mathematical structure, which fits into the form given in Eq. (1). Eliminating time explicitly from the primary creep and reformulating the creep rate in the form of strain hardening, the model's equations become as shown below.

$$f_{1p}(\sigma) = A_1 \sigma_{\theta}^{n_1}, \quad (7)$$

$$f_{1s}(\sigma) = A_2 [\sinh(a_0 \sigma_{\theta})]^{n_2}, \quad (8)$$

$$f_{2p}(T) = \exp(-Q_1 / T), \quad (9)$$

$$f_{2s}(T) = \exp(-Q_2 / T), \quad (10)$$

$$f_{3p}(\varepsilon) = v \exp[-\varepsilon_{\theta}^p / (f_{1p} f_{2p} A_p)], \quad (11)$$

$$f_{3s} \equiv 1, \quad (12)$$

$$A_p(\psi) = C_1 + C_2 \exp(-\lambda_1 \psi), \quad (13)$$

$$A_s(\psi) = 1 - \lambda_2 \psi, \quad (14)$$

The fluence term,  $A_s$ , in the CEA-EDF Model-2, Gras [7], has the following exponential form

$$A_s(\psi) = C_3 + C_4 \exp(-\lambda_3 \psi) \quad (15)$$

The numerical values for the model parameters can be obtained from the cited references.

**Modeling of Irradiation-Damage Annealing:** Irradiation-damage annealing can be introduced by calculating an effective fast fluence value from an annealing model and then using this value as input to the model. Depending on the temperature and time-at-temperature, this approach can result in totally eliminating the effects of both the fast fluence and the hydrogen on the creep rate, thereby reducing the creep rate to that of unirradiated material. However, since the effect of hydrogen is not recoverable, we cannot apply irradiation-annealing models directly without first isolating the effect of hydrogen from fast fluence in the creep model.

**Separation of Hydrogen Effect from Fluence Effect:** This is done by deriving a hydrogen dependent multiplier  $A(H)$  that is similar to, and takes the place of, the fluence-dependent multiplier  $A(\psi)$  shown in Eqs 13, 14 and 15. This is accomplished using data from Bouffieux and Rupa [9], which gives ratios of the secondary creep rate of hydrided to as-received unirradiated samples. An exponential best-fit was applied to this data as given in Table 1, which shows the experimentally determined ratios as well as the ratios obtained from the best-fit equation shown below.

$$A(H) = a \exp(bH), a = 0.883, b = -0.00153, H \leq 750 \text{ ppm}, \quad (16)$$

where  $H$  is the total hydrogen concentration including the hydrogen in solid solution. The parameters  $a$  and  $b$  in the above expression may be functions of temperature, but the data is not sufficient to prescribe a temperature dependence. It is relevant to note that creep experiments from Bouffieux and Legras [10] show similar trend at a temperature of 470°C. A creep-rate factor of 0.38 is derived from this data for hydrogen concentration in the range of 720-760 ppm, which is in general agreement with the best-fit value shown in Table I for hydrogen concentrations typical of high-burnup cladding.

Table I. Creep Rate Ratio Hydrided/As-Received Based on Ref. 9 Data

Temperature (°C)	Stress (MPa)	Hydrogen (PPM)	Creep Rate Ratio	
			Data	Best Fit
350	200	175	0.575	0.675
400	350	215	0.500	0.635
400	350	360	0.280	0.510
400	140	560	0.240	0.375

The above expression is incorporated in the model as a multiplier on the total creep rate. However, since the effects of hydrogen is already included implicitly in the irradiated creep data used for model calibration, the hydrogen multiplier is invoked only if irradiation annealing begins to reduce the effective fluence causing the creep rate to approach that of as-received material at full recovery. To prevent this condition, the model algorithm compares the numerical values of  $A(\psi)$  and  $A(H)$  and selects the smaller of the two as the multiplier. Thus, for fully annealed irradiation damage, the creep rate reverts to that of hydrided material. Irradiation-damage annealing is incorporated in the FALCON code through the MATPRO data base [11], which returns an effective fluence value as function of time. The effective fast fluence is computed from the following formula,

$$\psi = 10^{20} (2.49 \times 10^{-6} * t * e^{-5.35 \times 10^{23} / T^8} + 10^{20} / \psi_0)^{-1}, \quad (17)$$

where  $\psi_0$  and  $\psi$  are the fluence ( $n/m^2$ ) at the beginning and the end of the isothermal time step respectively,  $t$  is the time step size (s), and  $T$  is the temperature (K). We should caution, however, that recent annealing data indicate that the MATPRO annealing model gives somewhat faster irradiation damage annealing than observations. In the creep analysis of spent fuel rods under storage conditions, to be presented later, the hydrogen concentration is brought into the model through the following empirical relationship derived from data presented by Mardon et al. [12].

$$H = 35e^{0.051Bu} \quad (18)$$

where  $Bu$  is burnup in units of GWd/tU and  $H$  is in ppm.

## IMPLEMENTATION IN FUEL BEHAVIOR CODE AND MODEL VALIDATION

Model-3, modified for hydrogen effects and irradiation annealing, was implemented in the EPRI fuel behavior code FALCON [13]. The creep model and its host code were subjected to benchmarking and validation analysis using creep experiments conducted in the CEA/EDF program.

Validation cases include as-received, irradiated and hydrided CWSR materials with various stress and temperature conditions. The hydrogen sub-model  $A(H)$  was substituted for the irradiation hardening multiplier  $A(\psi)$  in the analysis of the hydrided data. FALCON results for the irradiated and hydrided data are shown in Fig. 1. As can be observed, the FALCON results slightly over-predict the irradiated data. This was intentionally done, by using lower input values for the effective fast fluence, to make the model predict the data from above to ensure conservative extrapolation to long term creep. The FALCON results for the hydrided samples are in reasonably good agreement with the data, particularly for hydrogen concentrations relevant to high burnup.

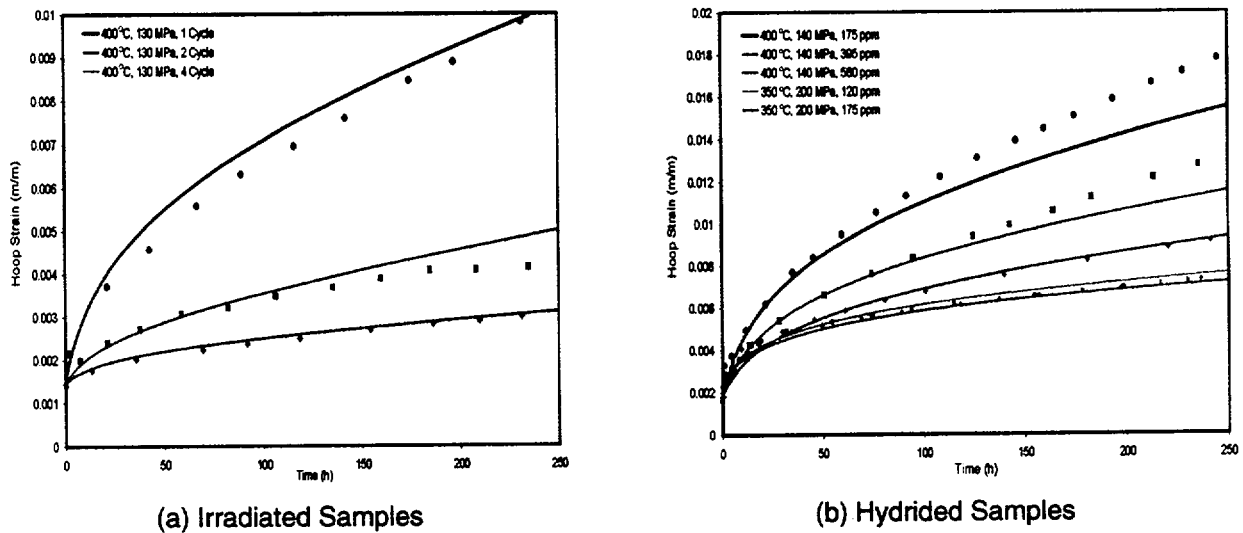


Figure 1. Validation of CEA/EDF Model-in-FALCON for Irradiated and Hydrided Materials

## ANALYSIS OF CREEP RUPTURE TESTS AND IMPLICATION TO ACCEPTANCE CRITERIA

In a closed-tube constant-pressure creep test, the stress is continuously changing with time according to the following relationship,

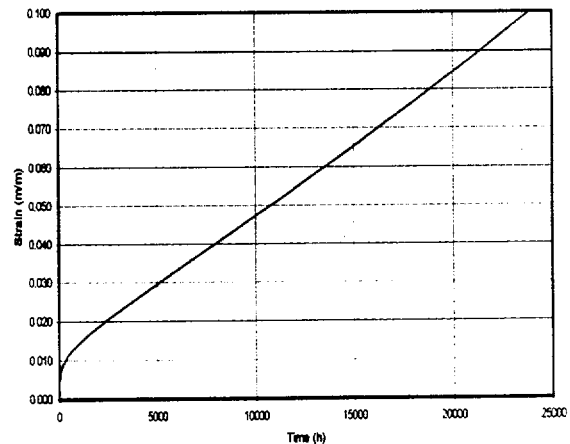
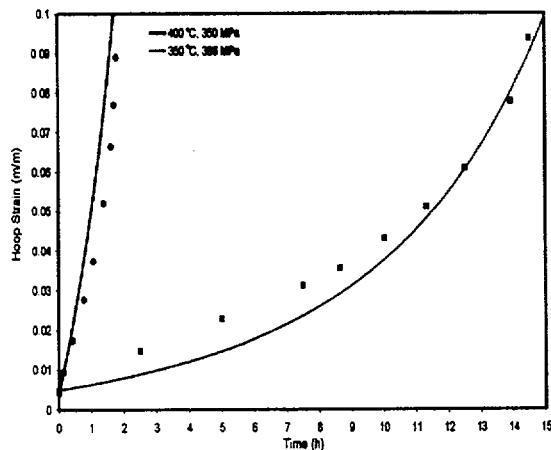
$$\sigma_{\theta\theta} = \sigma_{\theta_0} / (2e^{-\varepsilon_{\theta\theta}} - 1), \quad (19)$$

where  $\sigma_{\theta\theta}$  and  $\varepsilon_{\theta\theta}$  are, respectively, the hoop stress and hoop strain in the deformed tube and  $\sigma_{\theta_0}$  is the initial hoop stress in the un-deformed tube. In FALCON, the stress input to the creep model is converted to the equivalent initial stress using the above formula before substitution into the model. In low-stress short-term creep tests, the change in stress is small and can be neglected. For example, a 2% hoop

strain would cause the hoop stress to increase by about 4%, which is too small to introduce a noticeable change in the creep deformations. However, continued straining could eventually raise the stress above the yield strength, thereby initiating the tertiary creep regime, which progresses relatively quickly to rupture. This behavior is difficult to duplicate in the laboratory because of the very long testing time required. The alternative is to conduct accelerated creep tests by one of the following methods: increasing the temperature, increasing the stress, or both. Increasing the temperature is undesirable because of the activation of recrystallization and recovery processes. On the other hand, increasing the stress would not appreciably shorten the testing time unless the stress level is raised above the material's yield strength, which initiates the test in the tertiary regime and renders it invalid for judging cladding capacity under creep. This is because in the tertiary regime the accumulated strains are the result of plastic flow leading to failure by plastic instability. In this regard, accelerated creep tests differ from ordinary tensile tests only in the magnitude of the strain rate. Conventional creep tests, on the other hand, are initiated from a stress level well below the material's yield stress, (significantly below in the case of spent fuel), and they approach the tertiary creep stage from below at a strain rate that is smaller by more than six orders of magnitude. However, once the stress begins to rise above the yield stress, tertiary creep behavior begins to control the response as in the accelerated creep test. Extrapolation of such behavior to dry storage is further challenged by the fact that both the creep rate and rod pressure decline with time due to decreasing temperature.

To verify these findings, we have analyzed two CEA/EDF creep rupture tests: a 386MPa/350°C closed tube test and 350MPa/400°C axial test, Bouffioux and Rupa [9]. Both tests failed at a strain value of approximately 10%. FALCON's predictions of these tests are shown in Fig. 2, which shows good agreement with the measured strain up to the point of rupture. Using identical FALCON analysis procedure to that used for predicting the tests, we re-analyzed the test specimen starting from an initial stress of 200 MPa, which is well below the yield stress. The results are also depicted in Fig. 2. As can be seen, a 10% strain was reached after about 23,000 hours without any noticeable change in the creep rate or a tendency for tertiary behavior. Two important observations should be noted from these analyses. First, two deformation paths, both resulting in a strain of 10%, led to entirely different outcomes, proving the fact that strain is not a unique measure of material failure. Second, under a continuously decreasing stress with time, creep rupture would be virtually impossible in dry storage, even considering local wall thinning due to oxide spallation and hydriding.

It is clear from these results that there is an inherent deficiency in the process of using a strain limit as the sole measure of cladding integrity under creep, and therefore we must re-examine the approach of prescribing acceptance criteria based on strain alone. It is possible to incorporate in the analytical model local effects such as wall thinning due to oxidation and hydriding in the form of an enhanced initial stress and its subsequent evolution with time. Current regulatory restrictions placed on the oxide thickness, properly evaluated, can be shown to be totally unnecessary, and can be replaced by adding to the strain criterion a side condition on the hoop stress to remain below the unirradiated yield strength.



(a) CEA/EDF Creep Rupture Tests

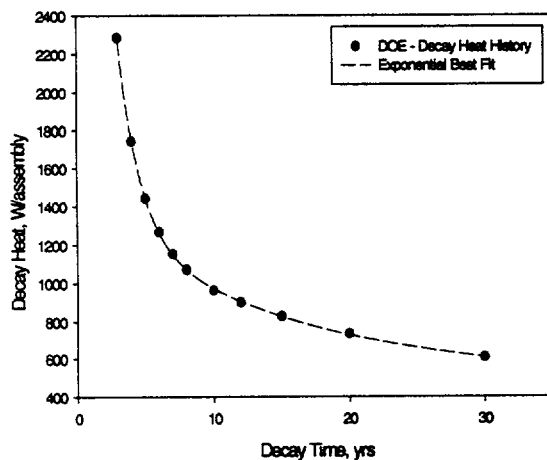
(b) Creep Response – 200 MPa Initial Stress

Figure 2 – FALCON Prediction of Creep Rupture Tests Compared to Normal Creep to 10% Strain

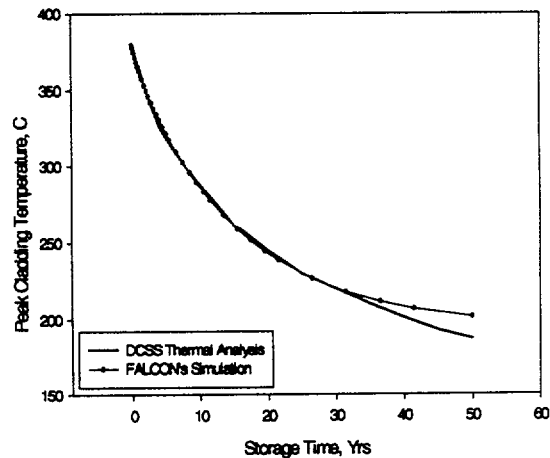
## APPLICATION TO DRY STORAGE

The creep methodology described above deals with a spent fuel rod isolated from the cask and the surrounding assemblies. In general applications, the thermal analysis of the dry cask storage system (DCSS) provides the thermal history for the governing fuel rod in the cask, which is then used as input to FALCON. In the present analysis, however, the fuel rod thermal history is calculated in FALCON using the decay-power curve for a 9-year cooled, 60 GWd/MtU rod. The FALCON calculations use a constant heat transfer coefficient, with axially varying profile. The heat transfer coefficient and ambient temperature values were obtained by conducting trial-and-error analyses until the calculations matched known DCSS thermal history, as shown in Fig. 3.

Using an initial temperature of 365°C and an initial stress of 138 MPa, a coupled thermal and creep analysis of a 17x17 geometry was performed using two geometric representations. The first analysis used a full-length R-Z model of the fuel rod with a reduced clad thickness equivalent to 120µm oxide. The temperature and pressure histories at the rod mid-height were transferred to an R-θ model with a locally thinned section to 50% of as-received thickness representing the presence of a hydride lens. The results for both geometries are depicted in Fig. 4. As can be observed, the creep strain in the thin section remains below 2% and the stress continues to decrease with time.



(a) Decay Power



(b) Cladding Temperature

Figure 3. FALCON Simulation of High Burnup Fuel Rod After 9 Years Cooling Time

## CONCLUSIONS

The application of a creep analysis methodology, consisting of a robust post-irradiation thermal creep model implemented in a state-of-the-art fuel behavior code, to spent fuel in dry storage shows that the current regulatory acceptance criteria can be relaxed considerably without compromising the safety, or the retrievability of spent fuel. An analysis of creep rupture tests and their simulations under dry storage conditions show that a fairly liberal strain criterion of several percent strain, combined with a side

condition on stress evolution with time to remain below the unirradiated yield strength, provide adequate protection against creep-induced failure.

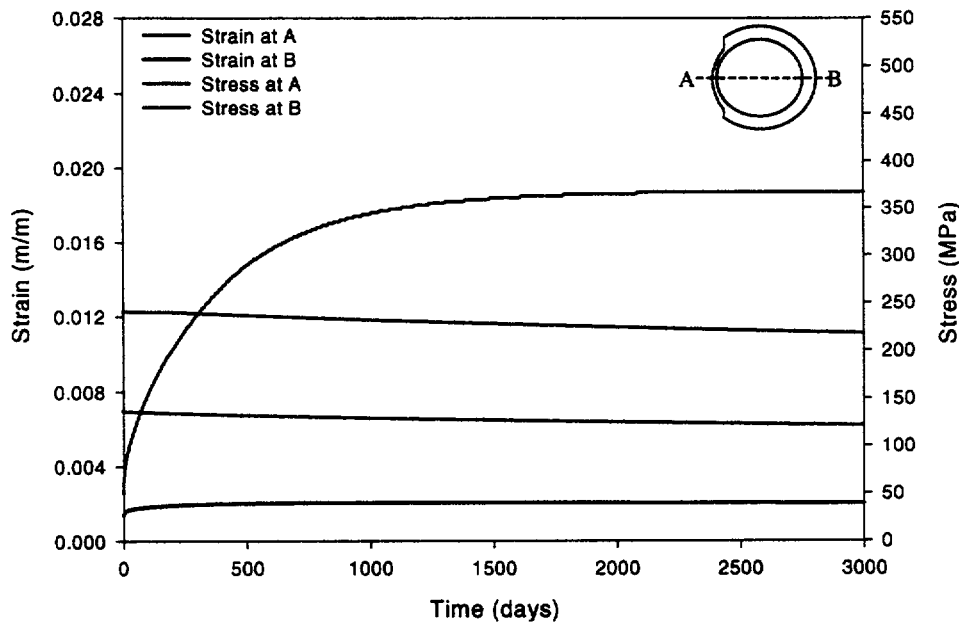


Figure 4. Creep Response of a Spent Fuel Rod with 120µm Oxide and Hydride Lens

## REFERENCES

1. Garde, A. M., Smith, G. P., and Pirek, R. C., ASTM STP 1295, 1996, pp. 407-430.
2. Fuketa et al, LWR Fuel Performance Meeting, Park City, Utah, April 10-13, 2000.
3. MATPRO-Version 11 (Rev. 2), EG&G Idaho, Inc., Department of Energy, NUREG/CR-0497, TREE-1280, Rev. 2, August, 1981.
4. Rashid, et al., "Creep as the Limiting Mechanism for Spent Fuel Dry Storage", EPRI ID # 1001207, December, 2000.
5. Franklin, et al., "Creep of Zirconium Alloys in Nuclear Reactors", ASTM STP 815, 1985.
6. Limon, et al., "A Formulation of the Spent Fuel Cladding Creep Behavior for Long Term Storage", LWR Fuel Performance Meeting, Park City, Utah, April 10-13, 2000.
7. Gras, J. M., "Entreposage Des Combustibles Usés", BILAN DU PPRD T4-97-07, EDF, Janvier 2000.
8. Bouffioux, Pol, "Interim Dry Storage of PWR's Spent Fuel – Development of a Creep Law to Assess the Fuel Cladding Integrity", ICEM01 Conf., Bruges, Belgium, Sept. 30 – Oct. 4, 2001.
9. Bouffioux, P. and Rupa, N., "Impact of Hydrogen on Plasticity and Creep of Unirradiated Zircaloy-4 Cladding Tubes", ASTM STP 1354, pp 399-422.
10. Bouffioux, P. and Legras, L., "Effect of Hydriding on the Residual Cold Work Recovery and Creep of Zircaloy 4 Cladding Tubes", LWR Meeting, Park City, Utah, April 10-13, 2000.
11. MATPRO-Version 11 (Rev. 2), EG&G Idaho, Inc., Department of Energy, NUREG/CR-0497, TREE-1280, Rev. 2, August, 1981.



12. Mardon, et al., "Influence of Composition and Fabrication Process on Out-of-Pile and In-Pile Properties of M5 Alloy", ASTM STP 1354, pp 505-524.
13. Montgomery, R.O., et. al., "FALCON Fuel Analysis and Licensing Code, Vol. 2, User's Manual," ANA-97-0230, ANATECH Corp., San Diego, California, December 1997.

## **Attachment 3**

---

# **Creep Rupture Analysis Comparison of FALCON to ABAQUS**

## Purpose

Creep rupture analyses produced by the FALCON code, presented during the NEI/NRC Meeting on April 18, 2001, were questioned by PNNL staff regarding the ability of computer codes to predict creep rupture. This is not an unjustified reaction; the material modeling and computational problems involved in such highly non-linear behavior are quite complex, not to mention the demands on the analyst's skills and experience. Since the FALCON code is used as the computational tool for the development of dry storage creep methodology, much would depend on gaining technical confidence of the NRC and PNNL staff in the capability of the code. To this end, we have undertaken an effort to compare the FALCON code to a general-purpose finite element code that is well known for its non-linear capabilities, namely, ABAQUS [1].

## Procedure

There are several main characteristics that make it possible for the code to calculate creep rupture, regardless of whether it is finite-element based or finite-difference based code. These are:

- (a) Ability to treat deformation-induced geometric non-linearities, i.e., finite strain theory
- (b) Ability to treat rate dependent plasticity (viscoplasticity).
- (c) Constitutive formulation that can account for the evolution of time-dependent stresses and the material's elastic-plastic properties.
- (d) Valid creep model and elastic plastic properties.

The first task in this effort was to develop the necessary software to input the creep model and the elastic-plastic properties of the cladding material through the UMAT user subroutine provided in ABAQUS. The material models utilized are the MATPRO elastic-plastic properties and a modified EDF/CEA creep model. Once the UMAT subroutine was constructed and verified, the code's input structure was utilized to complete the analysis input. The material properties were identical for both FALCON and ABAQUS. Both codes have the finite strain capabilities, but they could differ in the internal construction of the constitutive relations. For example, FALCON employs a rate-dependent viscoplasticity formulation, whereas ABAQUS treats plasticity as time independent. This difference could affect the accuracy of the calculations (FALCON's approach should be the more accurate), but not in whether or not creep rupture is calculable.

The cases analyzed are as follows:

400°C, 350 MPa, compared to data

350°C, 386 MPa, compared to data

400°C, 250 MPa, as a special case to illustrate the effect of plasticity on creep rupture prediction.

The following material describes the EDF/CEA creep model, the UMAT Fortran subroutine and the ABAQUS input decks.

### EDF/CEA (Bouffioux) Cladding Creep Model

The EDF/CEA creep model [2] for post-irradiation creep is expressed as follows:

$$\epsilon_{\text{eff}}^c = \epsilon_0(\sigma_{\text{eff}}, T) f_\epsilon(\phi) \ln(1 + c_1 t) + K(\sigma_{\text{eff}}, T) f_K(\phi) t, \quad (1)$$

where  $\epsilon_{\text{eff}}^c$  is the cladding effective creep strain (m/m),

$$\epsilon_0 = c_2 \sigma_{\text{eff}}^{c_3} e^{-c_4/T}, \quad (2)$$

$$K = c_5 e^{-c_7/T} [\sinh(c_8 \sigma_{\text{eff}})]^{c_6}, \quad (3)$$

$$f_\epsilon(\phi) = c_9 + c_{10} e^{-c_{11}\phi}, \quad (4)$$

$$f_K(\phi) = 1 - c_{12}\phi, \quad (5)$$

$\sigma_{\text{eff}}$  is the cladding effective stress in Pa,  $T$  is the temperature in K,  $\phi$  is the fast fluence in  $\text{n/m}^2$ , and  $c_1, c_2, c_3, c_4, c_5, c_6, c_7, c_8, c_9, c_{10}, c_{11}, c_{12}$  are constants fit to creep data.

In use this model in analysis, it is necessary to recast the creep rate in the form of strain hardening law. To this end, let

$$\epsilon_{\text{eff}}^{\text{c}_p} = \epsilon_0 f_\epsilon(\phi) \ln(1 + c_1 t), \quad (6)$$

where  $\epsilon_{\text{eff}}^{\text{c}_p}$  is the cladding effective *primary* creep strain. Then

$$\ln(1 + c_1 t) = \epsilon_{\text{eff}}^{\text{c}_p} / \epsilon_0 f_\epsilon(\phi), \quad (7)$$

and

$$1 + c_1 t = e^{\epsilon_{\text{eff}}^{\text{c}_p} / \epsilon_0 f_\epsilon(\phi)}. \quad (8)$$

Taking the time derivative of (1) and using (8), the creep rate becomes

$$\dot{\epsilon}_{\text{eff}}^{\text{c}} = c_1 \epsilon_0 f_\epsilon(\phi) e^{-\epsilon_{\text{eff}}^{\text{c}_p} / \epsilon_0 f_\epsilon(\phi)} + K f_K(\phi). \quad (9)$$

Note that in the EDF/CEA development, Equation (1) was used to define the *hoop creep strain*. However, it was implemented as an effective strain/effective stress formulation, to maintain compatibility with the continuum basis of the analysis method. As described in Reference 3, Attachment 2 to the RAI response, this model was modified to introduce the effects of annealing and hydrogen. This modification is included in the FORTRAN coding of the EDF/CEA model listed in this document.

### MATPRO-11 Stress-Strain Equation

The MATPRO stress-strain equation in the plastic regime can be expressed as:

$$\sigma_{\text{eff}} = e(\sigma_y / E + \epsilon_{\text{eff}})^n (\dot{\epsilon}_{\text{eff}} / \dot{\epsilon}_0)^m K, \quad (10)$$

where  $\sigma_y$  is the yield stress,  $E$  is Young's modulus,  $\epsilon_{\text{eff}}$  is the effective *inelastic* strain,  $\dot{\epsilon}_{\text{eff}}$  the effective inelastic strain rate,  $\dot{\epsilon}_0$  is a reference strain rate =  $1.E-3$ , and  $K, n,$  and  $m$  are material constants

that are functions of temperature, fluence, cold work, annealing, etc. fit to material property test data as defined by MATPRO.

Equation (9) was used to define the creep behavior and Equation (10) was used to describe the plasticity of the cladding. To these two equations we must add the elastic relation.

### **ABAQUS Creep Rupture Predictions Compared to FALCON**

Figure 1 shows the ABAQUS and FALCON results for the EDF/CEA 350°C-386MPa closed tube creep rupture test. The FALCON and ABAQUS predictions are plotted against the measured creep rupture data. Both the FALCON and ABAQUS predictions are seen to be in good agreement with the measured data. The ABAQUS prediction does not agree as well with the data, except for the prediction of the time to rupture (~15 hours).

Figure 2 shows the FALCON and ABAQUS results for the EDF/CEA 400°C-350MPa uniaxial creep test. The FALCON and ABAQUS predictions are plotted against the data. For this case, the FALCON prediction is seen to be in very good agreement with the data, and the ABAQUS prediction is seen to over predict the rupture time.

The curve in Figure 2, labeled "Enhanced Strain Hardening" is obtained by slightly stiffening the stress-plastic-strain curve in ABAQUS to determine the reason for ABAQUS' over-prediction of rupture time in comparison to FALCON and the data. It was determined that this was due to the time-independent plasticity formulation in ABAQUS, whereas FALCON treats plastic flow as rate dependent, as mentioned earlier.

Figure 3 shows ABAQUS predictions for a cladding tube at 400°C subjected to an initial uniaxial stress of 250 MPa. The purpose of this analysis is to demonstrate that creep rupture is a state of plastic instability. Figure 3 shows two predictions. In the first, we arbitrarily set the yield strength at 250 MPa, which is the same as the applied stress. In the second, the yield strength was set at 350 MPa. Both analyses are with 250 MPa applied stress. The response for the lower 250 MPa yield stress is initiated in the tertiary creep regime whereas, the response for the 350 MPa yield stress is almost *entirely elastic creep*, because plasticity is not reached until the strain exceeded 30%, at which time creep rupture becomes imminent. As can be seen, for the same applied stress creep rupture would occur at different times. This is just a simple example to illustrate the effect of plastic flow on creep rupture behavior, which should be kept in mind when extrapolating strains measured in creep rupture tests to creep behavior under lower stresses typical of dry storage.

### **Summary and Conclusions**

The analysis exercise described herein demonstrates that, given the right capabilities in the code, creep rupture can be predicted. It turned out that FALCON's capabilities in this regard are on par or better than ABAQUS, which is regarded as the standard of the state of the art in computational mechanics.

### **References**

1. **ABAQUS**, Version 5.8, Hibbitt, Karlsson & Sorensen, Inc., 1080 Main St., Pawtucket, RI 02860-4847

2. Cappelaere, C., Limon, R., Bdedel, T., Berat, L., CEA; Gilbon, D., *DRN/DMT/SEMI*; Bouffioux, P., *EDF*; Mardon, J. *Framatome*, The 8<sup>th</sup> International Conference on Environmental Management, Sept 30-October 4, 2001, Bruges, Belgium.
3. Rashid, J. Y. R., and Machiels, A. J., "Creep as the Limiting Mechanism of Spent Fuel in Dry Storage", The 8<sup>th</sup> International Conference on Environmental Management, ICEM01, Sept. 30-Oct. 4, 2001, Bruges, Belgium.

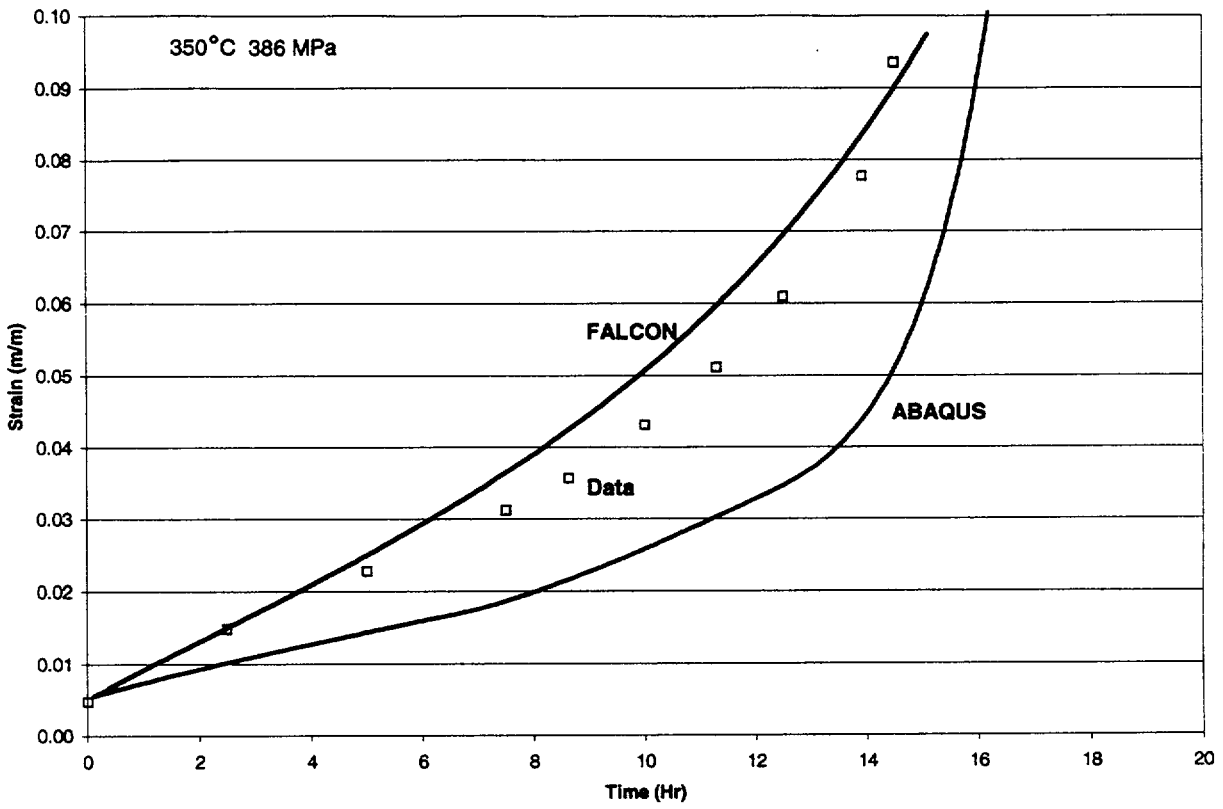


Figure 1. 350°C / 386 MPa FALCON Creep Rupture Validation by ABAQUS

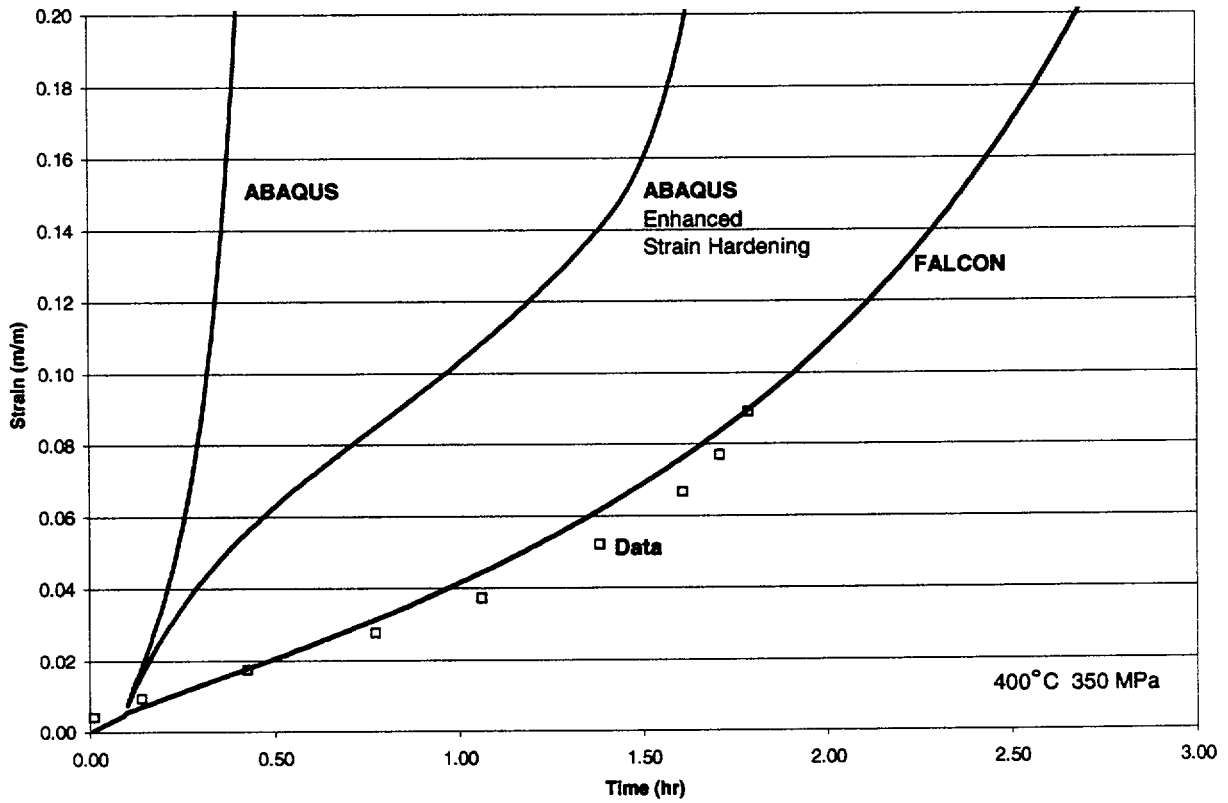


Figure 2. 400°C / 350 MPa FALCON Creep Rupture Validation by ABAQUS

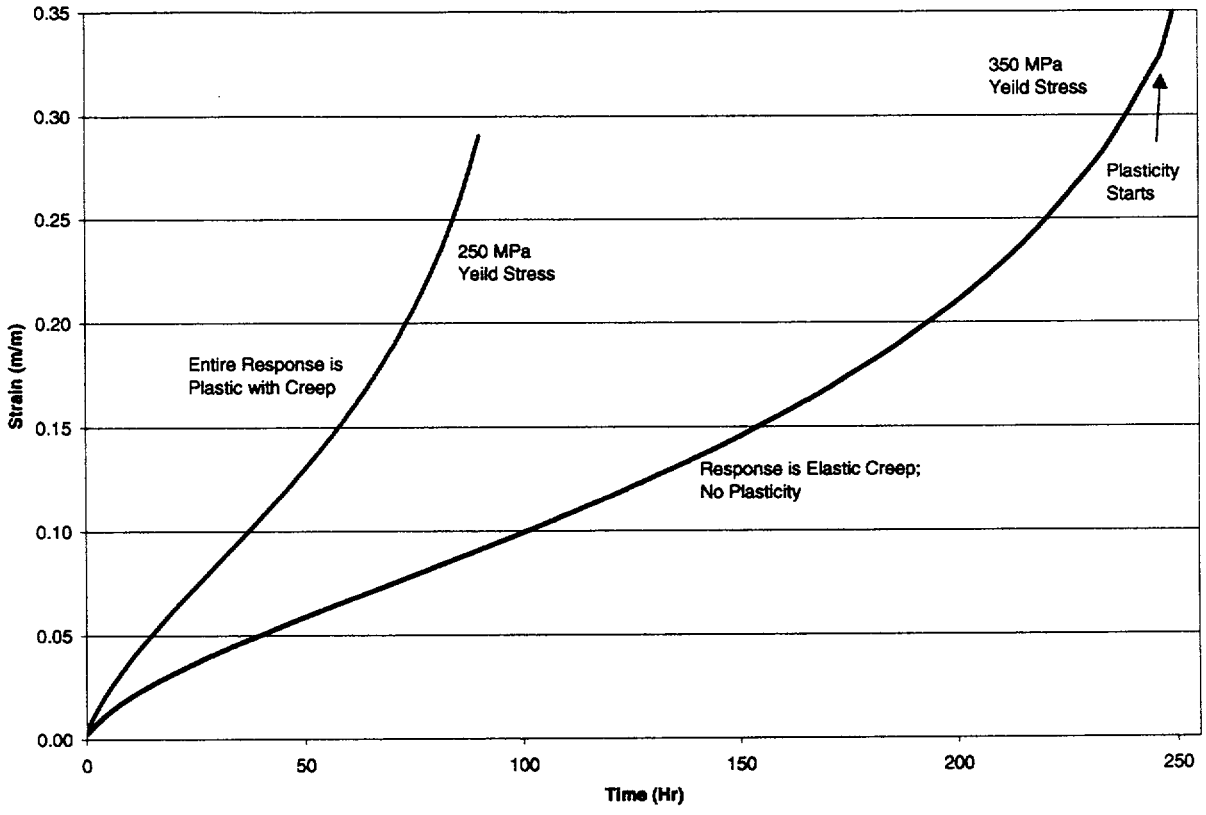


Figure 3. 400°C / 250 MPa ABAQUS Hypothetical Creep Rupture With & Without Plasticity



# **ABAQUS User Material Model Subroutine**

**Based on**

**Bouffioux, et al. Creep Model  
And Isotropic Strain Hardening Plasticity**

```

* * * * *
*          UMATBOU: Bouffieux Viscoplastic Constitutive Models          *
*          Copyright 2001 ANATECH Corp.                                *
* No part of this computer program (software) may be reproduced in    *
* any form or distributed in any way without prior written agreement   *
* with ANATECH Corp.                                                  *
*          ALL RIGHTS RESERVED                                         *
* * * * *
SUBROUTINE UMAT (STRESS, STATEV, HH, SSE, SPD, SCD,
$ RPL, DDSDDT, DRPLDE, DRPLDT,
$ TEPS, DEP, TIMEAB, DTIME, TEMP, DTEMP, PREDEF, DPRED, CMNAME,
$ NDI, NSHR, NTENS, NSTATV, PROPS, NPROPS, COORDS, DROT, PNEWDT,
$ CELENT, DFGRD0, DFGRD1, NOEL, NPT, LAYER, KSPT, KSTEP, KINC)
C
C      IMPLICIT DOUBLE PRECISION (A-H,O-Z)
C
C      Bouffieux creep model, NSTATV=5
C
C      STATEV(1)=Eff plastic strain
C      STATEV(2)=Flag
C      STATEV(3)=Eff primary creep strain
C      STATEV(4)=Eff total creep strain
C      STATEV(5)=RSTRAN
C
C      Required units:
C      Stress      Pa
C      Strain      m/m
C      Temperature K
C      Time        Hr
C
C      THE FOLLOWING ARE ABAQUS COMMON BLOCKS
C
C      COMMON /COUNT/ ICOUNT(4), ACOUNT(6), JCOUNT(6), BCOUNT, KCOUNT(2),
$ CCOUNT(3), LCOUNT(2), DCOUNT(4), MCOUNT(8), ECOUNT(4), NCOUNT(2),
$ FCOUNT(3), ICNT(4), GCOUNT(4), JCNT(2), HCOUNT, KCNT(4)
COMMON /CONTRO/ ICONTR(114)
C
C      PARAMETER (MAXMAT=100, NSV=5, NOUT=7, MAXCRV=100, OP5=1.5D0)
C
C...v...1...v...2...v...3...v...4...v...5...v...6...v...7..
C
C      COMMON /FLTNUM/ ZERO, HALF, ONE, TWO, THREE, TEN, PI, PIFAC
C
C      THE FOLLOWING ARE ABAQUS DIMENSIONS
C
C      CHARACTER CMNAME*(*)
C      DIMENSION STRESS(*), STATEV(*), HH(NTENS, NTENS), DDSDDT(*), DRPLDE(*),
$ TEPS(*), DEP(*), TIMEAB(*), PREDEF(*), DPRED(*), PROPS(*), COORDS(*),
$ DROT(3,*), DFGRD0(3,*), DFGRD1(3,*)
C
C      THE FOLLOWING ARE ANATECH DIMENSIONS
C
C      DIMENSION DEPS(6), YCRV(2, MAXCRV), H(6, 6), STROLD(6)
C
C      CHARACTER QDATE*9, QTIME*8, MATNAM(MAXMAT)*8
C
C      LOGICAL FIRSTE, MATPR, DEBUG
C
C      SAVE /FLTNUM/, INCRM0, JELNO1, NUMMAT, MATNAM, INT1, NSEC1, LAYER1
C

```

```

DATA FIRSTE/.TRUE./,JELNO1,INT1,NSEC1,LAYER1/4*0/
C
C           SET CONTROL PARAMETERS FROM ABAQUS
C
LDYNAB=ICONTR(5)
LARGE=ICONTR(2)
KSTFAB=KCOUNT(1)
JELNO=NOEL
INT=NPT
NSEC=KSPT
INCRAB=KINC
NSTPAB=KSTEP
TIME=TIMEAB(2)
C
C           SET DEBUG FLAG
C
CALL ANADBG(JELNO,INT,INCRAB,NSTPAB,COORDS,.FALSE.,.FALSE.,
$ FIRSTE,DEBUG)
C
C           FIRST TIME IN SUBROUTINE INITIALIZATION
C
IF (FIRSTE) THEN
  CALL FLOATN
  CALL DATTIM(QDATE,QTIME)
  JELNO1=JELNO
  INT1=INT
  NSEC1=NSEC
  LAYER1=LAYER
  FIRSTE=.FALSE.
  DO MAT=1,MAXMAT
    MATNAM(MAT)=' '
  ENDDO
  NUMMAT=0
  WRITE(NOUT,50)
50  FORMAT(/,' Bouffieux Viscoplastic Constitutive Model, ',
$ 'July 9,2001:',/,
$ ' No part of this computer program (software) may be',
$ ' reproduced in any form',/, ' or distributed in',
$ ' any way without prior written agreement.',/,
$ ' Copyright 2001 ANATECH Corp. ALL RIGHTS RESERVED')
  ENDIF
C
IF (JELNO.EQ.JELNO1.AND.INT.EQ.INT1.AND.NSEC.EQ.NSEC1.AND.
$ LAYER.EQ.LAYER1) THEN
  IF (NSTPAB.EQ.1.AND.INCRAB.EQ.1) THEN
    INCRMT=1
  ELSE
    INCRMT=2
  ENDIF
ENDIF
C
IF (DEBUG) WRITE(NOUT,30) JELNO,INT,NSTPAB,INCRAB,KSTFAB,TIME,
$ DTIME
30  FORMAT('UMAT: JELNO,INT,NSTPAB,INCRAB,KSTFAB,TIME,DTIME=',5I5,
$ 1P,2E11.3)
IF (STATEV(2).NE.ONE) INCRMT=1
C
C           STORE MATERIAL NAMES AND NUMBERS AND SET FLAG FOR FIRST
C           TIME MATERIAL PROPERTY PRINT
C

```

```

MATPR=.FALSE.
IF (INCRMT.EQ.1) THEN
  IF (NUMMAT.GE.MAXMAT) GO TO 100
  DO MAT=1,NUMMAT
    MATERL=MAT
    IF (CMNAME.EQ.MATNAM(MATERL)) GO TO 100
  ENDDO
  NUMMAT=NUMMAT+1
  MATERL=NUMMAT
  MATNAM(MATERL)=CMNAME
  MATPR=.TRUE.
ENDIF

C
100 IF (NSV.GT.NSTATV) THEN
  WRITE(NOUT,110) NSTATV,NSV
110  FORMAT('***TOO FEW STATE VARIABLES (DEPVAR) FOR THIS MODEL. ',
$ I2,' WERE DEFINED, AND ',I2,' ARE NEEDED.')
  STOP 'TOO FEW STATE VARIABLES (DEPVAR) TO UMATBOU'
  ELSEIF (NSV.LT.NSTATV.AND.MATPR) THEN
  WRITE(NOUT,120) NSTATV,NSV
120  FORMAT('***ATTENTION: TOO MANY STATE VARIABLES (DEPVAR) FOR ',
$ 'THIS MODEL. ',I2,' WERE DEFINED, BUT ONLY ',I2,
$ ' ARE NEEDED.')
  ENDF

C
C  Material Properties
C
  IF (NPROPS.LT.3) THEN
  WRITE(NOUT,130) NPROPS
130  FORMAT('***TOO FEW NPROPS TO UMATBOU: NPROPS = ',I5)
  STOP 'TOO FEW NPROPS TO UMATBOU'
  ENDF
  XVC=PROPS(1)
  YIELD=PROPS(2)
  IF (NPROPS.GE.3) THEN
  DELOXY=PROPS(3)
  ELSE
  DELOXY=ZERO
  ENDF
  IF (NPROPS.GE.4) THEN
  FNCK=PROPS(4)
  ELSE
  FNCK=ZERO
  ENDF
  IF (NPROPS.GE.5) THEN
  CWKF=PROPS(5)
  ELSE
  CWKF=ZERO
  ENDF
  IF (NPROPS.GE.6) THEN
  CHORG=PROPS(6)
  ELSE
  CHORG=ZERO
  ENDF
  IF (NPROPS.GE.7) THEN
  RSDAT=PROPS(7)
  ELSE
  RSDAT=ZERO
  ENDF
  IF (NPROPS.GE.8) THEN

```

```

    NCRV=NEAR (PROPS (8))
ELSE
    NCRV=0
ENDIF
C
RS=MAX (STATEV (5), 1.D-5)
DO I=1, NTENS
    STROLD (I) =STRESS (I)
    DEPS (I) =DEP (I)
    RS=MAX (RS, ABS (DEP (I)) /DTIME)
    DO J=1, NTENS
        H (J, I) =ZERO
    ENDDO
ENDDO
C
IF (RSDAT.GT.ZERO) THEN
    RSTRAN=MAX (RSDAT, 1.D-5)
ELSE
    RSTRAN=RS
ENDIF
RSTRAN=MIN (RSTRAN, TEN)
STATEV (5) =RSTRAN
CTEMP=TEMP+DTEMP/TWO
ELMOD=CELMOD (TEMP, FNCK, CWKF, DELOXY)
IF (MATPR) THEN
    WRITE (NOUT, 140) QDATE, QTIME, CMNAME, XVC, ELMOD, CTEMP, DELOXY, FNCK,
$   CWKF, CHORG, RSDAT
140  FORMAT ('UMATBOU Viscoplasticity Model', 2X, A9, 1X, A8, /,
$   'CMNAME = ', A8, /, 'XVC=', 0P, F7.3, /, 'ELMOD=', 1P, E11.3, ' Pa', /,
$   'CTEMP=', 0P, F7.1, ' K', /, 'DELOXY=', 1P, E11.3, /, 'FNCK=', 1P, E11.3, /,
$   'CWKF=', 0P, F7.3, /, 'CHORG=', 1P, E11.3, /, 'RSDAT=', 1P, E11.3)
    IF (NPROPS.LT. (2*NCRV+8)) THEN
        WRITE (NOUT, 150) NPROPS, NCRV
150    FORMAT ('***TOO FEW PROPERTIES. NPROPS=', I3, ' NCRV=', I3)
        STOP 'TOO FEW PROPERTIES TO UMATBOU'
    ELSEIF (NPROPS.GT. (2*NCRV+8)) THEN
        WRITE (NOUT, 160) NPROPS, NCRV
160    FORMAT ('***ATTENTION: TOO MANY PROPERTIES. NPROPS=', I3,
$   ' NCRV=', I3)
    ENDIF
ENDIF
NCRV=NCRV+1
YCRV (1, 1) =ZERO
YCRV (2, 1) =YIELD
NP=8
DO N=2, NCRV
    NP=NP+1
    YCRV (1, N) =PROPS (NP)
    NP=NP+1
    YCRV (2, N) =PROPS (NP)
ENDDO
IF (MATPR) WRITE (NOUT, 170) ((YCRV (I, N), I=1, 2), N=1, NCRV)
170  FORMAT ('Isotropic Hardening Curve', /, '      Strain      Yield',
$ /, (1P, 2E11.3))
C
C   Compute elastic strain-stress & stress-strain matrices
C
C1=-XVC/ELMOD
C2=ONE/ELMOD
DO I=1, NDI

```

```

DO J=1,NDI
  H(J,I)=C1
ENDDO
H(I,I)=C2
ENDDO
C3=(ONE+XVC)/ELMOD
N=NDI
DO I=1,NSHR
  N=N+1
  H(N,N)=C3
ENDDO
DO I=1,NTENS
  DO J=1,NTENS
    HH(J,I)=H(J,I)
  ENDDO
ENDDO
IF (DEBUG) THEN
  WRITE(NOUT,180)
180  FORMAT('UMAT: H BEFORE INVERT')
  DO I=1,NTENS
    WRITE(NOUT,190) (H(I,J),J=1,NTENS)
190  FORMAT(1P,6E11.3)
  ENDDO
ENDIF
CALL INVERT(HH,NTENS,NTENS,DEBUG,NOUT)
IF (DEBUG) THEN
  WRITE(NOUT,200)
200  FORMAT('UMAT: HH AFTER INVERT')
  DO I=1,NTENS
    WRITE(NOUT,190) (HH(I,J),J=1,NTENS)
  ENDDO
ENDIF
C
EPSEFF=STATEV(1)
EPSEFO=EPSEFF
PCEPS=STATEV(3)
TCEPS=STATEV(4)
CALL GLDEFS(NDI,NSHR,STROLD,SIGMO,SIGFO)
CALL GLDYLD(YIELD0,EPSEFO,EPO,YCRV,NCRV,DEBUG,NOUT)
IF (SIGFO.GT.ONE) THEN
C
C  Compute Bouffieux creep strain components
C
  BURNUP=ZERO
  CALL BCREEP(CTEMP,TCEPS,PCEPS,SIGFO,FNCK,BURNUP,CHORG,DTIME,
$  DTCEPS,DEBUG,NOUT,JELNO,INT)
  DTCEPS=OP5*DTCEPS/SIGFO
  ELSE
  DTCEPS=ZERO
  ENDF
C
DO I=1,NTENS
  DEPS(I)=DEPS(I)-DTCEPS*STROLD(I)
ENDDO
C
C  Elastic prediction of trial stresses
C
CALL GLDEPR(NTENS,STROLD,HH,DEPS,STRESS)
IF (DEBUG) THEN
  WRITE(NOUT,210) (STRESS(I),I=1,NTENS)

```

```

210   FORMAT('UMAT AFTER ELAS. PRED. STRESS',/,1P,6E11.3)
      ENDIF
      CALL GLDEFS(NDI,NSHR,STRESS,SIGM,SIGEFF)
      STATEV(2)=ONE
      STATEV(3)=PCEPS
      STATEV(4)=TCEPS
      IF (DEBUG) WRITE(NOUT,220) KSTFAB,SIGEFF,YIELDO
220   FORMAT('UMAT: KSTFAB,SIGEFF,YIELDO=',I3,1P,2E11.3)
      C
      C   Elastic creep
      C
      IF (KSTFAB.LE.1.OR.SIGEFF.LT.YIELDO) RETURN
      C
      C   Plastic creep
      C
      CALL GOLDST(STRESS,H,DEPS,ELMOD,XVC,EPSEFF,SIGEFF,EPO,YIELDO,
$ NTENS,NDI,NSHR,YCRV,NCRV,NOUT,DEBUG)
      C
      STATEV(1)=EPSEFF
      RETURN
      END

      FUNCTION CELMOD(CTEMP, FNCK, CWKF, DELOXY)
      C
      C   Calculates Young's modulus for zircaloy
      C
      C   CTEMP   cladding temperature           (K)
      C   FNCK    effective fast fluence         (neutrons/m2)
      C   CWKF    effective cold work           (unitless)
      C   DELOXY  average oxygen concentration  (kg oxygen/kg zirc)
      C
      IMPLICIT DOUBLE PRECISION (A-H,O-Z)
      C
      C1=(1.16D11+CTEMP*1.037D8)*5.7015
      C2=1.0
      IF (FNCK.GT.1.0D22) C2=0.88*(1.0-ANAEXP(-FNCK/1.0D25))+
$ ANAEXP(-FNCK/1.0D25)
      C3=-2.6D10
      CELMOD=(1.088D11-5.475D7*CTEMP+C1*DELOXY+C3*CWKF)/C2
      IF (CTEMP.LT.1090.) GO TO 140
      WFOX=DELOXY+0.0012
      TAAB=1094.+WFOX*(-1.289D+3+WFOX*7.914D+5)
      IF (WFOX.LT.0.025) GO TO 100
      TAAB=1556.4+3.8281D+4*(WFOX-0.025)
100   TABB=392.46*((100.*DELOXY+0.1242807)**2+3.1417)
      IF (DELOXY.LT.4.7308937D-3) GO TO 110
      TABB=(100.*DELOXY+0.12)*491.157+1081.7413
110   CONTINUE
      IF (CTEMP.LT.TAAB) GO TO 140
      IF (CTEMP.GT.TABB) GO TO 120
      AMODL=(1.088D11-5.475D7*TAAB+C1*DELOXY+C3*CWKF)/C2
      AMODR=9.21D10-TABB*4.05D7
      CELMOD=AMODL+(CTEMP-TAAB)*(AMODR-AMODL)/(TABB-TAAB)
      GO TO 140
120   CELMOD=9.21D10-CTEMP*4.05D7
140   CONTINUE
      RETURN
      END

      SUBROUTINE GOLDST(STRESS,H,DEPS,ECONC,XVC,EPSEFF,SIGEFF,EPO,

```

```

      $ YIELDO,NTENS,NDI,NSHR,YCRV,NCRV,NOUT,DEBUG)
C
C   ANATECH Isotropic Hardening Plasticity Model
C
      IMPLICIT DOUBLE PRECISION (A-H,O-Z)
      COMMON /FLTNUM/ ZERO,HALF,ONE,TWO,THREE,TEN,PI,PIFAC,BIG,DUM
C
C...v....1...v....2...v....3...v....4...v....5...v....6...v....7...
C
      LOGICAL DEBUG
      PARAMETER (MAXITR=9,X32=1.5D0,X23=2.D0/3.D0,X43=4.D0/3.D0,
$ X92=4.5D0,X324=324.D0,X648=648.D0,SIX=6.D0,FOUR=4.D0,RFAC=1.01D0,
$ EIGHT=8.D0,X36=36.D0,EM9=1.D-9,EM3=1.D-3,DEMAX=1.D36,RLFAC=0.1D0)
      DIMENSION STRESS(*),H(6,6),DEPS(*),YCRV(2,*),EPSHAT(6)
C
C   Plastic increment
C
      XK3=ECONC/(ONE-TWO*XVC)
      G2=ECONC/(ONE+XVC)
      G=G2/TWO
      G3=THREE*G
      G3XK3=G3*XK3
210  IF (DEBUG) WRITE(NOUT,210) ECONC,XVC,XK3,G2,G,G3,G3XK3
      FORMAT('GOLDST: ECONC,XVC,XK3,G2,G,G3,G3XK3=',/,1P,7E11.3)
      EPSEFO=EPSEFF
      CRIT=EM3*YIELDO/ECONC/TEN
      CALL GLDEFB(NDI,NSHR,DEPS,DEBAR,DEBUG,NOUT)
      CRITP=MIN(CRIT,DEBAR*EM3)
      EPOE=MAX(EPO/ECONC,-HALF)
      FACP=ONE/(ONE+EPOE)
      DEBAR=FACP*DEBAR
      FMAX=MAX(DEBAR,CRIT)
220  IF (DEBUG) WRITE(NOUT,220) DEBAR,CRIT
      FORMAT('GOLDST: DEBAR,CRIT=',1P,2E11.3)
      IF (DEBUG) WRITE(NOUT,230)
230  FORMAT(' ITR      EPSEFO      EPSEFF      DE      DEPSP',
$ '      F      DFDEP      YIELD      EP')
      ITR=0
      IMIN=0
      DEMIN=ZERO
240  CONTINUE
      ITR=ITR+1
C
C   One-time (ITR=1) plasticity calculations
C
      IF (ITR.LE.1) THEN
C
C   Compute trial strains
C
      DO I=1,NTENS
          SUM=ZERO
          DO J=1,NTENS
              SUM=SUM+H(I,J)*STRESS(J)
          ENDDO
          EPSHAT(I)=SUM
      ENDDO
C
      IF (NDI.EQ.3) THEN
C
C   3-D effective trial strain

```



```

C
EHVOL=ZERO
DO I=1,NDI
  EHVOL=EHVOL+EPSHAT(I)
ENDDO
EHVOL3=EHVOL/THREE
EHAT=ZERO
DO I=1,NDI
  EHAT=EHAT+(EPSHAT(I)-EHVOL3)**2
ENDDO
N=NDI
DO I=1,NSHR
  N=N+1
  EHAT=EHAT+HALF*(EPSHAT(N)**2)
ENDDO
EHAT=SQRT(X32*EHAT)
G2EHAT=G2*EHAT
DESPM=DEMAX
DEPSP=DEBAR
EPSEFF=EPSEFO+DEPSP
FMIN=YIELDO
ELSEIF (NDI.EQ.2) THEN

```

```

C
C Plane stress effective trial strain
C

```

```

  EHV2D=ZERO
  EH2D2=ZERO
  DO I=1,NDI
    EHV2D=EHV2D+EPSHAT(I)
    EH2D2=EH2D2+EPSHAT(I)**2
  ENDDO
  EHV2D2=EHV2D**2
  N=NDI
  DO I=1,NSHR
    N=N+1
    EH2D2=EH2D2+HALF*(EPSHAT(N)**2)
  ENDDO
  DESPM=TWO*DEBAR
  DEPSP=DEBAR
  EPSEFF=EPSEFO+DEPSP
  FMIN=YIELDO**2
  ELSEIF (NDI.EQ.1) THEN

```

```

C
C 1-D effective trial strain
C

```

```

  XK=XK3/THREE
  XK2=XK**2
  EHAT2=EPSHAT(1)**2
  GAM2=ZERO
  N=1
  DO I=1,NSHR
    N=N+1
    GAM2=GAM2+EPSHAT(N)**2
  ENDDO
  DESPM=TWO*DEBAR
  DEPSP=DEBAR
  EPSEFF=EPSEFO+DEPSP
  FMIN=YIELDO**2
ENDIF

```

```

C

```

```

C      Don't update effective plastic strain for small increments
C
      IF (DEBAR.LT.CRIT) THEN
          EPSEFF=EPSEFO
          GOTO 500
      ENDIF
      ENDIF
C
C      Newton increment in effective plastic strain
C
      CALL GLDYLD(YIELD,EPSEFF,EP,YCRV,NCRV,DEBUG,NOUT)
C
      IF (NDI.EQ.3) THEN
          F=YIELD-G2*EHAT+G3*DEPSP
          DFDEP=THREE*G+EP
C      IF (DEBUG) WRITE(NOUT,300) F,DFDEP
300    FORMAT('GOLDST: F,DFDEP=',1P,2E11.3)
      ELSEIF (NDI.EQ.2) THEN
          F1=ONE/G2+X32*DEPSP/YIELD
          F12=F1**2
          F2=XK3*F1
          F3=F2-ONE
          F32=F3**2
          F2=TWO+F2
          F22=F2**2
          SY2=YIELD**2
          DF1=X32*(YIELD-EP*DEPSP)/SY2
          F=(EH2D2-X23*F12*SY2)*F22+EHV2D2*(F32-THREE)
          DFDEP=TWO*(F2*EH2D2+F3*EHV2D2)*XK3*DF1-
$      X43*F1*F2*YIELD*(DF1*YIELD*(F2+XK3*F1)+F1*F2*EP)
      ELSEIF (NDI.EQ.1) THEN
          F1=ONE/G2+X32*DEPSP/YIELD
          F12=F1**2
          F4=SIX*XK*F1+ONE
          F42=F4**2
          SY2=YIELD**2
          DF1=X32*(YIELD-EP*DEPSP)/SY2
          F=X324*XK2*F12*EHAT2+THREE*F42*GAM2-FOUR*F42*F12*SY2
          DFDEP=X648*XK2*F1*DF1*EHAT2+X36*XK*F4*DF1*GAM2-EIGHT*F4*F1*
$      YIELD*(SIX*XK*F1*DF1*YIELD+F4*DF1*YIELD+F4*F1*EP)
      ENDIF
C
      AF=ABS(F)
      IF (IMIN.LE.0.OR.AF.LE.FMIN) THEN
          FMIN=AF
          IMIN=ITR
          DEMIN=DEPSP
      ENDIF
      IF (ITR.LE.MAXITR) THEN
          DE=-F/DFDEP
          DEPSP=DEPSP+DE
          IF (DEPSP.LT.ZERO) THEN
C
C      Use EPSEFO if DEPSP.LT.ZERO
C
          EPSEFF=EPSEFO
          ITR=MAXITR+1
          IF (NDI.LT.3) GOTO 240
          GOTO 500
          ENDIF

```

```

C      DEPSP=MIN(DEPSP,DEPSPM)
      EPSEFF=EPSEFO+DEPSP
      ENDIF
      IF (DEBUG) WRITE(NOUT,410) ITR,EPSEFO,EPSEFF,DE,
$ DEPSP,F,DFDEP,YIELD,EP
410   FORMAT(I3,1P,9E11.3)
C
      TEST=ABS(DE)
      IF (TEST.LE.CRITP) GOTO 500
      IF (ITR.LT.MAXITR) GOTO 240
C
      IF (TEST.LE.TEN*CRIT) GOTO 500
      IF (ITR.EQ.MAXITR) THEN
        IF (IMIN.EQ.ITR) GOTO 500
        EPSEFF=EPSEFO+DEMIN
      ELSE
        GOTO 500
      ENDIF
      IF (NDI.LT.3) GOTO 240
C
C      Perform the return on the total stress if NDI.LT.3
C
500   CONTINUE
      CALL GLDYLD(YIELD,EPSEFF,EP,YCRV,NCRV,DEBUG,NOUT)
      RADFAC=YIELD/SIGEFF
      IF (RADFAC.GT.RFAC) THEN
        WRITE(NOUT,530) RFAC,ITR,EPSEFF,DEPSP,YIELD,RADFAC
530   FORMAT('***RADFAC > ',F4.2,' IN GOLDST: ITR/EPSEFF,',
$ 'DEPSP,YIELD,RADFAC=',I3,/,1P,5E11.3)
      ENDIF
C
      CALL GLDRR(RADFAC,NDI,NSHR,STRESS,SIGM,STROLD)
C
      RETURN
      END

      SUBROUTINE GLDRR(RADFAC,NDI,NSHR,STRESS,SIGM,STROLD)
C
C      J2 Radial Return
C
      IMPLICIT DOUBLE PRECISION (A-H,O-Z)
      COMMON /FLTNUM/ ZERO,HALF,ONE,TWO,THREE,TEN,PI,PIFAC,BIG,DUM
      DIMENSION STRESS(*),STROLD(*)
C
C...v...1...v...2...v...3...v...4...v...5...v...6...v...7...
C
      DO I=1,NDI
        IF (NDI.EQ.3) THEN
          STRESS(I)=SIGM+RADFAC*(STRESS(I)-SIGM)
        ELSE
          STRESS(I)=RADFAC*STRESS(I)
        ENDIF
      ENDDO
      N=NDI
      DO I=1,NSHR
        N=N+1
        STRESS(N)=RADFAC*STRESS(N)
      ENDDO
C
      RETURN

```

END

SUBROUTINE GLDEPR (NTENS, STROLD, HH, DEPS, STRESS)

C  
C  
C

Elastic Prediction of new Stress State

IMPLICIT DOUBLE PRECISION (A-H,O-Z)  
COMMON /FLTNUM/ ZERO, HALF, ONE, TWO, THREE, TEN, PI, PIFAC, BIG, DUM  
DIMENSION STROLD (\*), HH (NTENS, NTENS), DEPS (\*), STRESS (\*)

C  
C...v....1....v....2....v....3....v....4....v....5....v....6....v....7..  
C

DO I=1, NTENS  
SUM=ZERO  
DO J=1, NTENS  
SUM=SUM+HH (I, J) \*DEPS (J)  
ENDDO  
STRESS (I) =STROLD (I) +SUM  
ENDDO  
RETURN  
END

SUBROUTINE GLDEFB (NDI, NSHR, DEPS, DEBAR, DEBUG, NOUT)

C  
C  
C

Estimate the size of the effective strain increment

IMPLICIT DOUBLE PRECISION (A-H,O-Z)  
COMMON /FLTNUM/ ZERO, HALF, ONE, TWO, THREE, TEN, PI, PIFAC, BIG, DUM  
LOGICAL DEBUG  
DIMENSION DEPS (\*)

C  
C...v....1....v....2....v....3....v....4....v....5....v....6....v....7..  
C

EPSM=ZERO  
DO I=1, NDI  
EPSM=EPSM+DEPS (I)  
ENDDO  
IF (NDI.EQ.3) THEN  
EPSM=EPSM/THREE  
DEBAR= (DEPS (1) -EPSM) \*\*2+ (DEPS (2) -EPSM) \*\*2+ (DEPS (3) -EPSM) \*\*2  
ELSEIF (NDI.EQ.2) THEN  
EPSZ=-EPSM  
DEBAR=DEPS (1) \*\*2+DEPS (2) \*\*2+EPSZ\*\*2  
ELSEIF (NDI.EQ.1) THEN  
EPSZ=-EPSM/TWO  
DEBAR=DEPS (1) \*\*2+TWO\*EPSZ\*\*2  
ENDIF  
N=NDI  
DO I=1, NSHR  
N=N+1  
DEBAR=DEBAR+HALF\* (DEPS (N) \*\*2)  
ENDDO  
DEBAR=SQRT (TWO\*DEBAR/THREE)  
IF (DEBUG) WRITE (NOUT, 170) DEBAR  
170 FORMAT ('GLDEFB: DEBAR=', 1P, E11.3)  
C  
RETURN  
END

SUBROUTINE GLDEFS (NDI, NSHR, STRESS, SIGM, SIGEFF)

```

C
C   Compute the effective stress
C
      IMPLICIT DOUBLE PRECISION (A-H,O-Z)
      COMMON /FLTNUM/ ZERO,HALF,ONE,TWO,THREE,TEN,PI,PIFAC,BIG,DUM
      DIMENSION STRESS(*)
C
C...v...1...v...2...v...3...v...4...v...5...v...6...v...7...
C
      SIGM=ZERO
      DO I=1,NDI
        SIGM=SIGM+STRESS(I)
      ENDDO
C
      SIGM=SIGM/THREE
      IF (NDI.EQ.3) THEN
        SIGEFF=(STRESS(1)-SIGM)**2+(STRESS(2)-SIGM)**2+
$ (STRESS(3)-SIGM)**2
      ELSEIF (NDI.EQ.2) THEN
        SIGEFF=(STRESS(1)-SIGM)**2+(STRESS(2)-SIGM)**2+SIGM**2
      ELSE
        SIGEFF=(STRESS(1)-SIGM)**2+TWO*(SIGM)**2
      ENDIF
      N=NDI
      DO I=1,NSHR
        N=N+1
        SIGEFF=SIGEFF+TWO*(STRESS(N)**2)
      ENDDO
      SIGEFF=SQRT(THREE*SIGEFF/TWO)
C
      RETURN
      END

      SUBROUTINE GLDYLD(YIELD,EPSEFF,EP,YCRV,NCRV,DEBUG,NOUT)
C
C   Compute the yield stress
C
      IMPLICIT DOUBLE PRECISION (A-H,O-Z)
      COMMON /FLTNUM/ ZERO,HALF,ONE,TWO,THREE,TEN,PI,PIFAC,BIG,DUM
      LOGICAL DEBUG
      DIMENSION YCRV(2,*)
C
C...v...1...v...2...v...3...v...4...v...5...v...6...v...7...
C
      IF (DEBUG) THEN
C       WRITE(NOUT,10) NCRV,EPSEFF
10      FORMAT('GLDYLD: NCRV,EPSEFF=' I3,1P,E11.3)
C       WRITE(NOUT,30) ((YCRV(I,J),I=1,2),J=1,NCRV)
30      FORMAT(' YCRV',/, (1P,2E11.3))
      ENDIF
C
C   Yield based on linearly interpolated yield data
C
      YIELD=YCRV(2,1)
      IF (NCRV.GE.2) THEN
        EP=(YCRV(2,2)-YCRV(2,1))/YCRV(1,2)
        DO N=2,NCRV
          IF (EPSEFF.LE.YCRV(1,N)) THEN
            RATIO=(EPSEFF-YCRV(1,N-1))/(YCRV(1,N)-YCRV(1,N-1))
            YIELD=YCRV(2,N-1)+RATIO*(YCRV(2,N)-YCRV(2,N-1))
          ENDIF
        END DO
      END IF

```

```

        EP=(YCRV(2,N)-YCRV(2,N-1))/(YCRV(1,N)-YCRV(1,N-1))
        GOTO 200
    ENDIF
ENDDO
    YIELD=YCRV(2,NCRV)
ENDIF
EP=ZERO
C
200  CONTINUE
C    IF (DEBUG) WRITE(NOUT,210) YIELD,EP
210  FORMAT('GLDYLD: YIELD,EP=',1P,2E11.3)
    RETURN
    END

    SUBROUTINE INVERT(A,NDIM,NMAX,DEBUG,NOUT)
C
C...v...1...v...2...v...3...v...4...v...5...v...6...v...7...
C
    IMPLICIT DOUBLE PRECISION (A-H,O-Z)
    DIMENSION A(NDIM,NDIM)
    LOGICAL DEBUG
    PARAMETER (ZERO=0.0D0,ONE=1.0D0,BILL=1.0D9,DTOL=1.0D-30,
$ MAXERR=10)
    SAVE NERROR
    DATA NERROR/0/
C
    TOL=ZERO
    DO I=1,NMAX
        TOL=TOL+ABS(A(I,I))
    ENDDO
    TOL=TOL/NMAX/BILL
C
    DO N=1,NMAX
        D=A(N,N)
C
        IF (D.LE.TOL) THEN
            NERROR=NERROR+1
            IF (NERROR.GT.MAXERR) STOP 'BAD PIVOTS IN INVERT'
            WRITE(NOUT,60) D
60      FORMAT('***BAD PIVOT IN INVERT= ',1P,E11.3,' /MATRIX')
            DO I=1,NMAX
                WRITE(NOUT,65) (A(I,J),J=1,NMAX)
65      FORMAT(1P,12E11.3)
            ENDDO
            IF (ABS(D).LT.DTOL) STOP 'ZERO PIVOT IN INVERT'
        ENDIF
C
        DO J=1,NMAX
            A(N,J)=-A(N,J)/D
        ENDDO
        DO I=1,NMAX
            IF (N.NE.I) THEN
                DO J=1,NMAX
                    IF (N.NE.J) A(I,J)=A(I,J)+A(I,N)*A(N,J)
                ENDDO
            ENDIF
            A(I,N)=A(I,N)/D
        ENDDO
        A(N,N)=ONE/D
    ENDDO

```

```

C
RETURN
END

SUBROUTINE ANADBG(JELNO,INT,INCRAB,NSTPAB,COORDS,FSET,BUGSET,      .6 7/4/95
$ FIRST,DBUG)

C
IMPLICIT DOUBLE PRECISION (A-H,O-Z)
C
DIMENSION COORDS(*)
C
LOGICAL BUGSET,DEBUG,DBUG,FIRSTE,FIRST,FSET                      .6 7/4/95
C
SAVE DEBUG,FIRSTE
C
DATA DEBUG/.FALSE./, FIRSTE/.TRUE./
C
THIS BRANCH IS FOR USE BY PROGRAMS OTHER THAN UMAT, E.G., UMDRVR
C
IF (BUGSET.OR.FSET) THEN                                        .6 7/4/95
  IF (BUGSET) DEBUG=DBUG
  IF (FSET) FIRSTE=FIRST
ELSE
C
THIS BRANCH IS FOR USE BY UMAT AND CAN BE USED TO SET DEBUG AND
C
THE VARIOUS ANATECH PARAMETERS AS A FUNCTION OF JELNO, INT, ETC.
C
DEBUG=DEBUG
C
IF (JELNO.EQ.37.AND.INT.EQ.1.AND.INCRAB.EQ.4) DEBUG=.TRUE.
C
ENDIF
RETURN
END

SUBROUTINE FLOATN
IMPLICIT DOUBLE PRECISION (A-H,O-Z)
C
COMMON /FLTNUM/ ZERO,HALF,ONE,TWO,THREE,TEN,PI,PIFAC
C
ZERO=0.0D0
ONE=1.0D0
TWO=ONE+ONE
HALF=ONE/TWO
THREE=TWO+ONE
FOUR=TWO*TWO
FIVE=THREE+TWO
XNINE=THREE*THREE
TEN=TWO*FIVE
PIFAC=ATAN(ONE)
PI=PIFAC*FOUR
PIFAC=PIFAC/(XNINE*FIVE)
C
RETURN
END

SUBROUTINE DATTIM (QDATE,QTIME)
CHARACTER*(*) QDATE,QTIME
QDATE = ' '
QTIME = ' '

```

```

CALL DATE (QDATE)
CALL TIME (QTIME)
RETURN
END

```

```

SUBROUTINE NOCHAR (WORD, NCHAR)

```

```

C
C CHARACTER WORD* (*), BLNK*1
C
C REMOVE LEADING BLANKS
C
BLNK=' '
N=LEN (WORD)
IF (N.GT.0) THEN
  NBLNK=0
  DO I=1,N
    IF (WORD (I:I).NE.BLNK) GO TO 20
    NBLNK=NBLNK+1
  ENDDO
ENDIF
NCHAR=0
RETURN

```

```

C
20 NCHAR=N-NBLNK
WORD (:NCHAR)=WORD (NBLNK+1:N)

```

```

C
C REMOVE TRAILING BLANKS
C
N=NCHAR
DO I=1,N
  IF (WORD (NCHAR:NCHAR).NE.BLNK) GO TO 40
  NCHAR=NCHAR-1
ENDDO
40 RETURN
END

```

```

FUNCTION ANAEXP (X)
IMPLICIT DOUBLE PRECISION (A-H,O-Z)
COMMON /FLTNUM/ ZERO, HALF, ONE, TWO, THREE, TEN, PI, PIFAC

```

```

C
C...v...1...v...2...v...3...v...4...v...5...v...6...v...7...
C

```

```

PARAMETER (ARGMAX=80.D0)
IF (X.LT.-ARGMAX) THEN
  ANAEXP=ZERO
  RETURN
ELSEIF (X.GT.ARGMAX) THEN
  ANAEXP=ONE/ZERO
ELSE
  ANAEXP=EXP (X)
ENDIF
RETURN
END

```

```

FUNCTION NEAR (X)
IMPLICIT DOUBLE PRECISION (A-H,O-Z)
NEAR=NINT (X)
RETURN
END

```



## **EDF/CEA Bouffioux, et al. Creep Model**

```

SUBROUTINE BCREEP (CTEMP, TCEPS, PCEPS, QTILD, FNCK, BURRUP, CHORG, DTIME,
$ DTCEPS, DEBUG, NOUT, JELNO, INT)
C
C Required units:
C Stress Pa
C Strain m/m
C Temperature K
C Time Hr
C
C IMPLICIT DOUBLE PRECISION (A-H,O-Z)
C
C . . . . .1 . . . . .2 . . . . .3 . . . . .4 . . . . .5 . . . . .6 . . . . .7 . . .
COMMON /FLTNUM/ ZERO, HALF, ONE, TWO, THREE, TEN, PI, PIFAC
LOGICAL DEBUG
DIMENSION C(12)
SAVE C
DATA C/0.132D0, 20867.2D-2, 1.986D0, 13748.D0, 1.386D12, 1.715D0,
$ 27628.7D0, 0.01453D0, 0.065D0, 0.935D0, 5.708D-22, 1.102D-22/
C
C . . . . .1 . . . . .2 . . . . .3 . . . . .4 . . . . .5 . . . . .6 . . . . .7 . . .
C . . . . .1 . . . . .2 . . . . .3 . . . . .4 . . . . .5 . . . . .6 . . . . .7 . . .
C
C COMMON /FLTNUM/ ZERO, HALF, ONE, TWO, THREE, TEN, PI, PIFAC
LOGICAL DEBUG
DIMENSION C(12)
SAVE C
DATA C/0.132D0, 20867.2D-2, 1.986D0, 13748.D0, 1.386D12, 1.715D0,
$ 27628.7D0, 0.01453D0, 0.065D0, 0.935D0, 5.708D-22, 1.102D-22/
C
FLUENC=FNCK/1.D4
FLUENC=MIN(8.5D+21, FLUENC)
STRES=QTILD/1.D6
SINSH=SINH(C(8)*STRES)
FE0=C(9)+C(10)*ANAEKP(-C(11)*FLUENC)
FKO=ONE-C(12)*FLUENC
H=9.94D4*ANAEKP(-4167.D0/CTEMP)
BU=MAX(BURRUP/86400.D0, ZERO)
BU=MIN(BU, 100.D0)
IF (BU.GT.ZERO) THEN
  HPPM=MAX(35.D0*ANAEKP(.051D0*BU), ZERO)
ELSE
  HPPM=ZERO
ENDIF
HPPM=MAX(HPPM, CHORG)
IF (HPPM.GT.ZERO) THEN
  HKO=.883D0*ANAEKP(-.00153D0*HPPM)
ELSE
  HKO=ONE
ENDIF
FKO=MIN(FKO, HKO)
FE0=MIN(FE0, HKO)
E01=C(2)*(STRES**C(3))*ANAEKP(-C(4)/CTEMP)
EK=C(5)*ANAEKP(-C(7)/CTEMP)*(SINSH**C(6))
PRATE=E01*FE0*C(1)*ANAEKP(-PCEPS/(E01*FE0))
PCEPS=PCEPS+PRATE*DTIME
SRATE=EK*FKO
TRATE=PRATE+SRATE
DTCEPS=TRATE*DTIME
TCEPS=TCEPS+DTCEPS
IF (DEBUG) WRITE (NOUT, 10) TCEPS, PCEPS, QTILD, DTIME, CTEMP, DTCEPS
FORMAT('BCREEP: TCEPS, PCEPS, QTILD, DTIME, CTEMP, DTCEPS=', //,
$ 1P, 7E11.3)
C
RETURN
END

```

## **INPUT FILES FOR ABAQUS**

## Input File for ABAQUS 350°C / 386 MPa Creep Rupture Prediction

```
*HEADING
ab350_386p_zb.inp 1-element uniaxial const pressure creep rupture
*NODE,NSET=ALLNODES
1, 1.0, 0.0
2, 1.005, 0.0
3, 1.01, 0.0
4, 1.0, 0.5
5, 1.01, 0.5
6, 1.0, 1.0
7, 1.005, 1.0
8, 1.01, 1.0
*ELEMENT,TYPE=CAX8,ELSET=ONE
1, 1,3,8,6,2,5,7,4
*SOLIDSECTION,ELSET=ONE,MATERIAL=ZIRC
*MATERIAL,NAME=ZIRC
*USERMATERIAL,CONSTANTS=16
0.425, 394.4E6, 0.0, 0.0, 0.115, 0.0, 1.E-4, 4.0
8.796E-3,4.018E8, 8.699E-2,4.165E8, 1.456E-1,4.205E8, 1.945E-1,4.228E8
*DEPVAR
5
*NSET,NSET=BC0
1,2,3
*BOUNDARY
BC0, 2,2, 0.0
*EQUATION
2
6,2,-1.0, 7,2,1.0
2
8,2,-1.0, 7,2,1.0
2
4,1,-1.0, 1,1,1.0
2
6,1,-1.0, 1,1,1.0
2
5,1,-1.0, 3,1,1.0
2
8,1,-1.0, 3,1,1.0
*INITIAL CONDITIONS,TYPE=TEMPERATURE
ALLNODES, 623.15
*RESTART,WRITE,FREQUENCY=1
*STEP,NLGEOM,INC=20
*STATIC,DIRECT=NOSTOP
0.005,0.1
*CONTROLS,ANALYSIS=DISCONTINUOUS
*CONTROLS,PARAMETER=TIME INCREMENTATION
,,12
*DLOAD
1, P4, 3.86E6
*ELPRINT,FREQUENCY=1,TOTALS=NO,SUMMARY=NO
*NODEPRINT,FREQUENCY=1,TOTALS=NO,SUMMARY=NO
*ELFILE,FREQUENCY=1
S
SINV
E
SDV
*NODEFILE,FREQUENCY=1
U
```

```
*END STEP
*STEP,NLGEOM,INC=750
*STATIC,DIRECT=NOSTOP
0.1,18.3
*CONTROLS,ANALYSIS=DISCONTINUOUS
*CONTROLS,PARAMETER=TIME INCREMENTATION
,,12
*END STEP
```

## Input File for ABAQUS 400°C / 350 MPa Creep Rupture Prediction With Unstable Default Strain Hardening Curve

```

*HEADING
ab400_350p_zb.inp 1-element uniaxial const pressure creep rupture
*NODE,NSET=ALLNODES
1, 1.0, 0.0
2, 1.005, 0.0
3, 1.01, 0.0
4, 1.0, 0.5
5, 1.01, 0.5
6, 1.0, 1.0
7, 1.005, 1.0
8, 1.01, 1.0
*ELEMENT,TYPE=CAX8,ELSET=ONE
1, 1,3,8,6,2,5,7,4
*SOLIDSECTION,ELSET=ONE,MATERIAL=ZIRC
*MATERIAL,NAME=ZIRC
*USERMATERIAL,CONSTANTS=18
0.425, 337.1E6, 0.0, 0.0, 0.08, 0.0, 1.E-4, 5.0
8.827E-3,3.443E8, 2.844E-2,3.505E8, 5.787E-2,3.551E8, 1.265E-1,3.604E8
1.952E-01,3.635E8
*DEPVAR
5
*NSET,NSET=BC0
1,2,3
*BOUNDARY
BC0, 2,2, 0.0
*EQUATION
2
6,2,-1.0, 7,2,1.0
2
8,2,-1.0, 7,2,1.0
2
4,1,-1.0, 1,1,1.0
2
6,1,-1.0, 1,1,1.0
2
5,1,-1.0, 3,1,1.0
2
8,1,-1.0, 3,1,1.0
*INITIAL CONDITIONS,TYPE=TEMPERATURE
ALLNODES, 673.15
*RESTART,WRITE,FREQUENCY=1
*STEP,NLGEOM,INC=40
*STATIC,DIRECT=NOSTOP
0.005,0.1
*CONTROLS,ANALYSIS=DISCONTINUOUS
*CONTROLS,PARAMETER=TIME INCREMENTATION
,,12
*DLOAD
1, P4, 3.5E6
*ELPRINT,FREQUENCY=1,TOTALS=NO,SUMMARY=NO
*NODEPRINT,FREQUENCY=1,TOTALS=NO,SUMMARY=NO
*ELFILE,FREQUENCY=1
S
SINV
E
SDV

```

```
*NODEFILE, FREQUENCY=1
U
*END STEP
*STEP, NLGEOM, INC=200
*STATIC, DIRECT=NOSTOP
0.01, 1.9
*CONTROLS, ANALYSIS=DISCONTINUOUS
*CONTROLS, PARAMETER=TIME INCREMENTATION
,,, 12
*END STEP
```

## Input File for ABAQUS 400°C / 350 MPa Creep Rupture Prediction With Enhanced Strain Hardening Behavior

```

*HEADING
ab400_350pc_zb.inp 1-element uniaxial const pressure creep rupture
*NODE,NSET=ALLNODES
1, 1.0, 0.0
2, 1.005, 0.0
3, 1.01, 0.0
4, 1.0, 0.5
5, 1.01, 0.5
6, 1.0, 1.0
7, 1.005, 1.0
8, 1.01, 1.0
*ELEMENT,TYPE=CAX8,ELSET=ONE
1, 1,3,8,6,2,5,7,4
*SOLIDSECTION,ELSET=ONE,MATERIAL=ZIRC
*MATERIAL,NAME=ZIRC
*USERMATERIAL,CONSTANTS=12
0.425, 340.E6, 0.0, 0.0, 0.08, 0.0, 1.E-4, 2.0
0.1,4.2E8, 0.2,4.5E8
*DEPVAR
5
*NSET,NSET=BC0
1,2,3
*BOUNDARY
BC0, 2,2, 0.0
*EQUATION
2
6,2,-1.0, 7,2,1.0
2
8,2,-1.0, 7,2,1.0
2
4,1,-1.0, 1,1,1.0
2
6,1,-1.0, 1,1,1.0
2
5,1,-1.0, 3,1,1.0
2
8,1,-1.0, 3,1,1.0
*INITIAL CONDITIONS,TYPE=TEMPERATURE
ALLNODES, 673.15
*RESTART,WRITE,FREQUENCY=1
*STEP,NLGEOM,INC=40
*STATIC,DIRECT=NOSTOP
0.005,0.1
*CONTROLS,ANALYSIS=DISCONTINUOUS
*CONTROLS,PARAMETER=TIME INCREMENTATION
,,12
*DLOAD
1, P4, 3.5E6
*ELPRINT,FREQUENCY=1,TOTALS=NO,SUMMARY=NO
*NODEPRINT,FREQUENCY=1,TOTALS=NO,SUMMARY=NO
*ELFILE,FREQUENCY=1
S
SINV
E
SDV
*NODEFILE,FREQUENCY=1

```



```
U
*END STEP
*STEP,NLGEOM,INC=200
*STATIC,DIRECT=NOSTOP
0.01,1.9
*CONTROLS,ANALYSIS=DISCONTINUOUS
*CONTROLS,PARAMETER=TIME INCREMENTATION
,,,12
*END STEP
```

## Input File for ABAQUS 400°C / 250 MPa Creep Rupture Prediction 350 MPa Yield

```
*HEADING
ab400_250_zc.inp 1-element axial const load creep rupture
*NODE,NSET=ALLNODES
1, 0.00474, 0.0
2, 0.00505, 0.0
3, 0.00536, 0.0
4, 0.00474, 0.0005
5, 0.00536, 0.0005
6, 0.00474, 0.001
7, 0.00505, 0.001
8, 0.00536, 0.001
*ELEMENT,TYPE=CAX8,ELSET=ONE
1, 1,3,8,6,2,5,7,4
*SOLIDSECTION,ELSET=ONE,MATERIAL=ZIRC
*MATERIAL,NAME=ZIRC
*ELASTIC
9.37E+10, 0.425
*CREEP,LAW=USER
*DEPVAR
2
*PLASTIC
 3.50E8, 0.0
 4.34E8, 0.15
*NSET,NSET=BC0
1,2,3
*BOUNDARY
BC0, 2,2, 0.0
*EQUATION
2
6,2,-1.0, 7,2,1.0
2
8,2,-1.0, 7,2,1.0
2
4,1,-1.0, 1,1,1.0
2
6,1,-1.0, 1,1,1.0
2
5,1,-1.0, 3,1,1.0
2
8,1,-1.0, 3,1,1.0
*INITIAL CONDITIONS,TYPE=TEMPERATURE
ALLNODES, 673.15
*RESTART,WRITE,FREQUENCY=1
*STEP,NLGEOM,INC=20
*STATIC
0.001,0.01,,0.001
*CLOAD
6, 2, 8.1971E2
7, 2, 3.2789E3
8, 2, 8.1971E2
*ELPRINT,FREQUENCY=1,TOTALS=NO,SUMMARY=NO
*NODEPRINT,FREQUENCY=1,TOTALS=NO,SUMMARY=NO
*ELFILE,FREQUENCY=1
S
SINV
E
PE
```

SDV  
\*NODEFILE, FREQUENCY=1  
U  
\*END STEP  
\*STEP, NLGEOM, INC=700  
\*VISCO, CETOL=0.01  
1.0, 6000., , 10.0  
\*END STEP